# Inverting passive margin stratigraphy for marine sediment transport dynamics over geologic time

**Charles M. Shobe[1,2,*], Jean Braun[2], Xiaoping Yuan[2,3], Benjamin Campforts[2,4], Boris Gailleton[2], Guillaume Baby[5], François Guillocheau[5], and Cécile Robin[5]**

[1]*Department of Geology and Geography, West Virginia University, Morgantown, WV, USA*

[2]*Helmholtz Centre Potsdam, GFZ German Research Centre for Geosciences, Potsdam, Germany*

[3]*School of Earth Sciences, China University of Geosciences, Wuhan, China*

[4]*Community Surface Dynamics Modeling System, Boulder, CO, USA*

[5]*University of Rennes, Rennes, France*

CMS (*corresponding author): charles.shobe@mail.wvu.edu
JB: jbraun@gfz-potsdam.de
XY: xyuan@gfz-potsdam.de
BC: benjamin.campforts@colorado.edu
BG: boris.gailleton@gfz-potsdam.de
FG: francois.guillocheau@univ-rennes1.fr
CR: cecile.robin@univ-rennes1.fr
GB: baby.guillaume@gmail.com

# Inverting passive margin stratigraphy for marine sediment transport dynamics over geologic time

**Charles M. Shobe[1,2,*], Jean Braun[2], Xiaoping Yuan[2,3], Benjamin Campforts[2,4], Boris Gailleton[2], Guillaume Baby[5], François Guillocheau[5], and Cécile Robin[5]**

[1]*Department of Geology and Geography, West Virginia University, Morgantown, WV, USA*

[2]*Helmholtz Centre Potsdam, GFZ German Research Centre for Geosciences, Potsdam, Germany*

[3]*School of Earth Sciences, China University of Geosciences, Wuhan, China*

[4]*Community Surface Dynamics Modeling System, Boulder, CO, USA*

[5]*University of Rennes, Rennes, France*

*corresponding author: charles.shobe@mail.wvu.edu

**ABSTRACT**

Passive margin stratigraphy contains time-integrated records of landscapes that have long since vanished. Quantitatively reading the stratigraphic record using coupled landscape evolution and stratigraphic forward models (SFMs) is a promising approach to extracting information about landscape history. However, the most commonly used SFM, which is based on an approximation of local, linear slope-dependent sediment transport, fails to produce diagnostic features of passive margin stratigraphy such as long-distance transport from the continental shelf and slope onto the abyssal plain. There is no consensus about the optimal form of simple SFMs because there has been a lack of direct tests against observed stratigraphy in well constrained test cases. Here we develop a nonlocal, nonlinear one-dimensional SFM that incorporates slope bypass and long-distance sediment transport, both of which have been previously identified as important model components but not thoroughly tested. Our model collapses to the local, linear model under certain parameterizations such that best-fit parameter values can be indicative of optimal model structure. Using seven detailed seismic sections from the South African Margin, we invert the stratigraphic data for best-fit model parameter values and demonstrate that best-fit parameterizations are not compatible with the local, linear diffusion model. Fitting the observed stratigraphy requires parameter values consistent with important contributions from slope bypass and long-distance transport processes. The nonlocal, nonlinear model yields improved fits to the data regardless of whether the model is compared against only the modern bathymetric surface or the full set of seismic reflectors identified in the data. Results suggest that processes of sediment bypass and long-distance transport are required to model realistic passive margin stratigraphy, and are therefore important to consider when inverting the stratigraphic record to infer past perturbations to source regions.

## INTRODUCTION

Reconstructing landscape evolution trajectories—and the environmental boundary conditions that governed them—from the geologic past is a key goal in geomorphology. Such reconstructions are challenging because erosion processes continually destroy past topography, leaving only minor traces of ancient landscapes (e.g., river terraces; Molnar et al., 1994; Schanz et al., 2018) from which to deduce past landscape boundary conditions. Fortunately, every source has its sink; all sediment eroded from a terrestrial drainage basin must go somewhere. The sedimentary record, in regions where it is preserved and where there exists plausible long-term connectivity between source and sink, therefore represents our best hope of inferring time-resolved records of landscape change and its tectonic and climatic drivers with reasonable accuracy and precision. One geologic setting with particularly high potential for the preservation of relatively complete records of terrestrial erosion is marine passive margin basins, which contain Earth's most complete archives of sediment sourced from adjacent, eroding terrestrial environments (e.g., Steckler et al., 1988; Allen and Allen, 2013).

Passive margin stratigraphy contains a time-resolved record that, under the right conditions, can be used to reconstruct past tectonic and climatic perturbations to Earth's surface (e.g., Poag and Sevon, 1989; Poag, 1992; Pazzaglia and Brandon, 1996; Baby et al., 2018; Ding et al., 2019a). While the stratigraphic record can suffer from signal buffering, stratigraphic incompleteness, and signal shredding (e.g., Sadler, 1981; Jerolmack and Paola, 2010; Straub et al., 2020), the variability that leads to these effects is thought to yield average behavior that can be predicted at passive margin evolution timescales (tens to hundreds of Ma), producing a record that reflects large-scale, long-lasting perturbations to landscapes provided that those perturbations have amplitudes and durations that exceed the background level of "noise" in the sedimentary system (Straub et al., 2020). Historically, efforts to read the stratigraphic record of passive margins have focused on the study of sediment thicknesses, volumes, textures, lithological/mineralogical makeup, and chemistry, which leads to interpretations about the history of terrestrial erosion dynamics (e.g., Poag and Sevon, 1989). As numerical stratigraphic forward models (SFMs) became more common (e.g., Steckler et al., 1993; 1996; Syvitski and Hutton, 2001; Burgess et al., 2006), stratigraphic modelers began to use inverse techniques to extract environmental forcing information from forward simulation of the stratigraphic record (e.g.,Lessenger and Cross, 1996; Cross and Lessenger, 1999; Bornholdt et al., 1999). The great potential of the stratigraphic record for revealing past landscape evolution has led to efforts to couple landscape evolution models (LEMs) and SFMs (e.g., Granjeon and Joseph, 1999; Salles and Hardiman, 2016; Salles et al., 2018; Ding et al., 2019a,b; Yuan et al., 2019a, Salles, 2019; Zhang et al., 2020; Mallard and Salles, 2021) to build full source-to-sink numerical models, and in some cases to use large ensembles of those models to directly invert observed stratigraphy for past perturbations on eroding continents (Yuan et al., 2019a). The idea underpinning such inversions is that misfit between observed and modeled stratigraphy can be minimized to reveal best-fit values for relevant forcing parameters such as rock uplift rate, assuming that the model is an accurate representation of erosion, transport, and deposition processes integrated over geologic time. The utility of coupled LEM/SFM approaches to reconstructing past landscape evolution is well-demonstrated both through direct inversion (Yuan et al., 2019a) and comparison of forward model results with stratigraphy (Ding et al., 2019a).

Previous efforts focused on margin spatial scales and ~100 Ma timescales have typically used an approach in which marine sediment transport is conceptualized as being linearly dependent on local bathymetric slope, which when combined with mass conservation yields a linear-diffusion-like model (e.g., Moretti and Turcotte, 1985; Kenyon and Turcotte, 1985; Rivenaes, 1992; 1997; Ross et al., 1994; Paola, 2000; Braun et al., 2013; Rouby et al., 2013; Yuan et al., 2019a; Ding et al., 2019a; Zhang et al., 2020). However, this approach might not be capable of producing large-scale stratal geometries that agree with observations. In the stratigraphy of many passive margin basins, we observe substantial accumulations of sediment hundreds of kilometers from shore on the continental rise and abyssal plain that must have bypassed the higher-gradient continental slope (Lowe, 1976; Syvitski et al., 1988) and then been transported long distances over negligible slopes on the basin floor (Talling et al., 2012, Luchi et al., 2018; Hereema et al., 2020). The sole dependence of sediment flux on local slope neglects both sediment transport over negligible slopes and the potential influence of nonlocal transport processes, or those processes for which the distribution of sediment travel distances is heavy-tailed such that some sediment moves long distances relative to the scale of the model grid (e.g., Foufoula-Georgiou et al., 2010). Transport dynamics are especially likely to deviate from local-slope dependent behavior when sediment particles are fine enough to be suspended in the water column as observed in turbidity currents and other marine mass flows (e.g., Parker et al., 1986; Mohrig et al., 1998). In a nonlocal conceptualization of downslope sediment transport, erosion or deposition at a point has some dependence on surface slope elsewhere (Furbish and Roering, 2013; Doane et al., 2018). Nonlocal processes like sediment plumes from river mouths, turbidity currents, marine landslides, and debris flows are responsible for much of the long-distance transport observed along passive margins and are therefore relevant for any model that seeks to simulate passive margin stratigraphy. Such processes and deposits may not be fully consistent with the assumptions or predictions of local, linear transport models because they may require nonlocal and/or nonlinear conceptualizations of sediment transport dynamics.

Substantial effort has been devoted to parameterizing large-scale terrestrial landscape evolution models (e.g., Guerit et al., 2019; Yanites et al., 2018; Barnhart et al., 2019; Barnhart et al., 2020a,b,c) and testing how well they predict landscape form (e.g., van der Beek and Bishop, 2003; Valla et al., 2010; DiBiase and Whipple, 2011; Hobley et al., 2011; Barnhart et al., 2020b), but the same is not true of seascape evolution models— numerical models that govern marine sediment transport and changes in bathymetry over basin evolution timescales. While there is no shortage of options (e.g., Steckler et al., 1993; Granjeon and Joseph, 1999; Paola, 2000; Salles et al., 2018; Thran et al., 2020), at this point it is unclear what mathematical form of simple, long-term/large-scale seascape evolution models best represents the development of passive margin stratigraphy as few have been explicitly tested against observed stratigraphy in well constrained test cases.

Here we test a generalized one-dimensional SFM that moves beyond local, linear diffusion by incorporating, as suggested by previous work, sediment transport dynamics that allow sediment to bypass steep bathymetric slopes and travel beyond the base of the continental slope. We test the applicability of this new model and the commonly used local, linear model by quantitative comparison against seismic stratigraphic data from well-studied passive margin basins along the Southeast Atlantic Margin (SAM), southern Africa. Results from model-data comparison indicate that, at least over ~100 Ma timescales, passive margin seascape evolution and the development of marine stratigraphy are inconsistent with the commonly used, local, linear model but are consistent with a model that incorporates nonlocal and nonlinear transport dynamics. This indicates that passive margin evolution and stratigraphy may be dominated by nonlocal, nonlinear sediment transport processes that may be critical ingredients in models used to invert passive margin stratigraphy for past terrestrial landscape evolution.

# MODELING SEASCAPE EVOLUTION OVER GEOLOGIC TIME

## Commonly Used Models

The classical approach to modeling seascape evolution (and therefore the way, by tracking the bathymetric surface through time, of modeling marine stratigraphy) is to use an analogy to the heat equation that yields a linear diffusion equation where bathymetric elevation $z$ is the variable “diffusing” over time and where the gradient driving diffusion is the bathymetric slope $\frac{\partial z}{\partial x}$ (Kenyon and Turcotte, 1985; Ross et al., 1994). The downslope sediment flux per unit contour length $q_s$ goes linearly with local bathymetric slope:

$$q_s = -K\frac{\partial z}{\partial x}, (1)$$

and the divergence of sediment flux sets the rate of bathymetric change:

$$\frac{\partial z}{\partial t} = \nabla q_s = K\frac{\partial^2 z}{\partial x^2}. (2)$$

Here *K*, assumed here for simplicity to be independent of time and space, is a transport coefficient that governs the rate of bathymetric diffusion. The key assumption in this approach is that downslope sediment flux goes linearly with the local bathymetric slope, such that no variables beyond *K* and bathymetry influence the rate of seascape evolution.

There is no clear physical basis for such a slope-dependent diffusion equation at low slopes (i.e., on the continental shelf) and shallow water depths (see Paola, 2000 for a review), and an *ad hoc* solution has been to assert that the diffusion rate constant declines with water depth *d* (e.g., Kaufman et al., 1992; van Balen et al., 1995) as wave- and storm-driven bed shear stresses are reduced:

$$K(d) = K_0 e^{-d/d_*}. (3)$$

Here $K_0$ is the diffusion rate constant at the water surface ($d = 0$) and $d_*$ is the e-folding depth scale that governs the decline in *K* with depth below the water surface. When $d_*$ is small relative to the total basin depth (i.e., when there are substantial declines in sediment transport efficiency with depth), the linear diffusion approach yields morphologies analogous to continental shelves, shelf breaks, and steeper continental slopes. Similar morphologic results are achieved by asserting that terrestrial sediment fluxes deposit at a fixed slope when they reach the shoreline and then become subject to marine sediment transport by linear diffusion (Yuan et al., 2019a). Linear diffusion models, with or without modifications in the shallow environment, deliver little sediment beyond the base of the continental slope because the governing equation asserts that the downslope sediment flux approaches zero as the local bathymetric slope approaches zero.

The inconsistency of pure linear diffusion models with observations of nonlocal transport and long-distance sedimentation has long been noted (e.g., Syvitski et al., 1988), and has motivated model modifications such as adding advective components of sediment transport (Niedoroda et al., 1995, Pirmez et al., 1998; Granjeon and Joseph, 1999; Thran et al., 2020), allowing sediment bypass on slopes above some angle (e.g., Lowe, 1976; Syvitski et al., 1988; Ross et al., 1994; Thran et al., 2020), and enforcing that only some (potentially slope-dependent) proportion of total sediment flux may be deposited at any given point, with the rest being routed downslope even if linear diffusion theory alone would predict negligible flux (Ding et al., 2019a, Thran et al., 2020). Here we generalize these ideas, as well as recent advances from terrestrial landscape evolution modeling, into a simple SFM that is rooted in diffusion theory but incorporates two key modifications to account for both transport over low slopes and nonlocal transport.

## A Modified Seascape Evolution Model

The modified model is a generalization of existing ideas for how seascape evolution might deviate from the local, linear model that (1) is simple enough to be applied over basin-filling timescales, (2) is parsimonious enough to allow iterative calibration of all parameters, and (3) collapses under certain parameter values to the local, linear model. The model is most intuitively cast in terms of a balance between the volumetric entrainment rate per unit bed area $E$ and volumetric deposition rate per unit bed area $D$ (e.g., Beaumont et al., 1992; Kooi and Beaumont, 1994; van Balen et al., 1995; Davy and Lague, 2009; Carretier et al., 2016; Shobe et al., 2017; Yuan et al., 2019b; Campforts et al., 2020; Braun, 2021). The statement of mass conservation that governs the change in bathymetry at a point can therefore be written:

$$\frac{\partial z}{\partial t} = -E + D. \quad (4)$$

This framework is convenient because both of the models we propose to compare—the local, linear model and the nonlocal, nonlinear model—can be represented by altering the functional forms of *E* and *D*. As shown by Carretier et al. (2016), assuming that the entrainment rate is linearly proportional to the local slope $\frac{\partial z}{\partial x}$:

$$E = -K\left|\frac{\partial z}{\partial x}\right|, (5)$$

and that the deposition rate is the volumetric sediment flux per unit width $q_s$ over the model grid cell spacing dx:

$$D = \frac{q_s}{dx}, (6)$$

yields the local, linear model with behavior identical to equation 2. Its two key assumptions are that sediment entrainment depends only on local slope and that the deposition rate depends only on the downslope sediment flux.

The nonlocal, nonlinear model uses equation 5 to calculate sediment entrainment but makes two key modifications relative to the local, linear model inspired by observations from passive margin depositional systems. These are intended to allow (1) a nonlinear dependence of sediment transport on local slope to account for the transition to mass failures and turbidity currents experienced at higher slopes as well as sediment bypass, or non-deposition, on slopes assumed to be unable to sustain further steepening beyond some critical slope at which frequent failures are generated, and (2) transport of sediment over negligible slopes as observed in data from deep marine deposits. The modified model rests heavily on recent advances in terrestrial and marine modeling, especially the framework proposed by Carretier et al. (2016) for modeling hillslope sediment transport.

Carretier et al. (2016) proposed altering equation 6 to encapsulate a nonlinear dependence of the deposition rate on slope such that sediment deposition declines as slope increases towards some imposed threshold (e.g., Andrews and Bucknam, 1987; Roering et al., 1999), such that:

$$D = \frac{q_s\left(1-\left(\left|{}^{(\partial z/\partial x)}/_{S_c}\right|\right)^2\right)}{dx}. \ (7)$$

Here $S_c$ is the critical slope, best thought of physically as the slope at or above which no further deposition can occur and all remaining sediment continues downslope. As discussed by Carretier et al. (2016), this model is therefore nonlocal in the sense that sediment supplied from upslope can continue downslope if the deposition rate is insufficient to disentrain all sediment. Similar approaches to sediment bypass have also been used in recent seascape evolution models (e.g., Thran et al., 2020).

Equation 7 has one feature that makes it less than suitable for modeling marine transport: at a slope of zero, all sediment in transport is deposited. This is not a problem encountered in the eroding hillslopes for which the model was developed (Carretier et al., 2016), but contradicts the observed behavior of marine sediment transport agents (e.g., marine debris flows and turbidity currents) that travel hundreds of km over negligible slopes. Because our goal is to simulate the integrated effects of such events over Ma to hundred-Ma timescales, it is important that our model have a mechanism for transport of sediment over negligible slopes.

To allow transport of sediment over near-zero slopes, we modify Carretier et al's (2016) model by adopting from Ding et al. (2019a) the idea that only some proportion of sediment in transport will be deposited at any given location. We incorporate this modification by altering equation 7 to:

$$D = \frac{q_s\left(1-\left(\left(\partial z/\partial x\right)/S_c\right)^2\right)}{\lambda}, \quad (8)$$

where $\lambda$ is a sediment transport length scale that is larger than the model grid cell spacing. When $\lambda >> dx$, only some small proportion of the amount of sediment in transport is deposited. The rest continues in transport towards the distal portion of the margin. When $\lambda = dx$, all sediment in transport is deposited. While this approach is heuristic, it allows for the model to incorporate the general sediment transport patterns thought to occur in the deep, distal portions of continental margins. Modeled sediment can travel long distances down the continental slope because entrainment is linearly proportional to slope (equation 5) and because deposition becomes negligible as slopes approach the critical slope of non-deposition. At the transition from the continental slope to the lower-gradient continental rise and abyssal plain, low slopes drive reduced sediment entrainment rates and increased deposition rates, but the condition $\lambda >> dx$ allows continued transport across the abyssal plain in lieu of direct calculations of debris flow/turbidity current momentum (e.g., Parker et al., 1986). The modified model allows an approximation of nonlocal transport in the sense that the amount of sediment deposited at a given distance from shore depends not only on the local slope at that point but on all the points upslope that have contributed sediment to—or removed it from—active transport.

At a point, the rate of elevation change responds to three key quantities: the entrainment coefficient $K$, the slope $\frac{\partial z}{\partial x}$ relative to the critical slope of non-deposition $S_c$, and the sediment transport length scale $\lambda$ (Figure 1). For a given $\lambda$, there is a shift from net deposition to net erosion as $\frac{\partial z}{\partial x}$ approaches $S_c$ as the deposition rate declines and the entrainment rate increases. At a given $\frac{\frac{\partial z}{\partial x}}{S_c}$, increasing $\lambda$ causes a shift towards less deposition (or more entrainment) as more sediment remains in transport and less is deposited. The $\frac{\frac{\partial z}{\partial x}}{S_c}$ at which there exists a shift from net deposition to net entrainment (i.e., a shift from positive $\frac{\partial z}{\partial t}$ to negative $\frac{\partial z}{\partial t}$) depends on $\lambda$. For $\frac{\frac{\partial z}{\partial x}}{S_c} > 1$, no deposition can occur, $\lambda$ ceases to matter, and entrainment continues to scale linearly with slope.

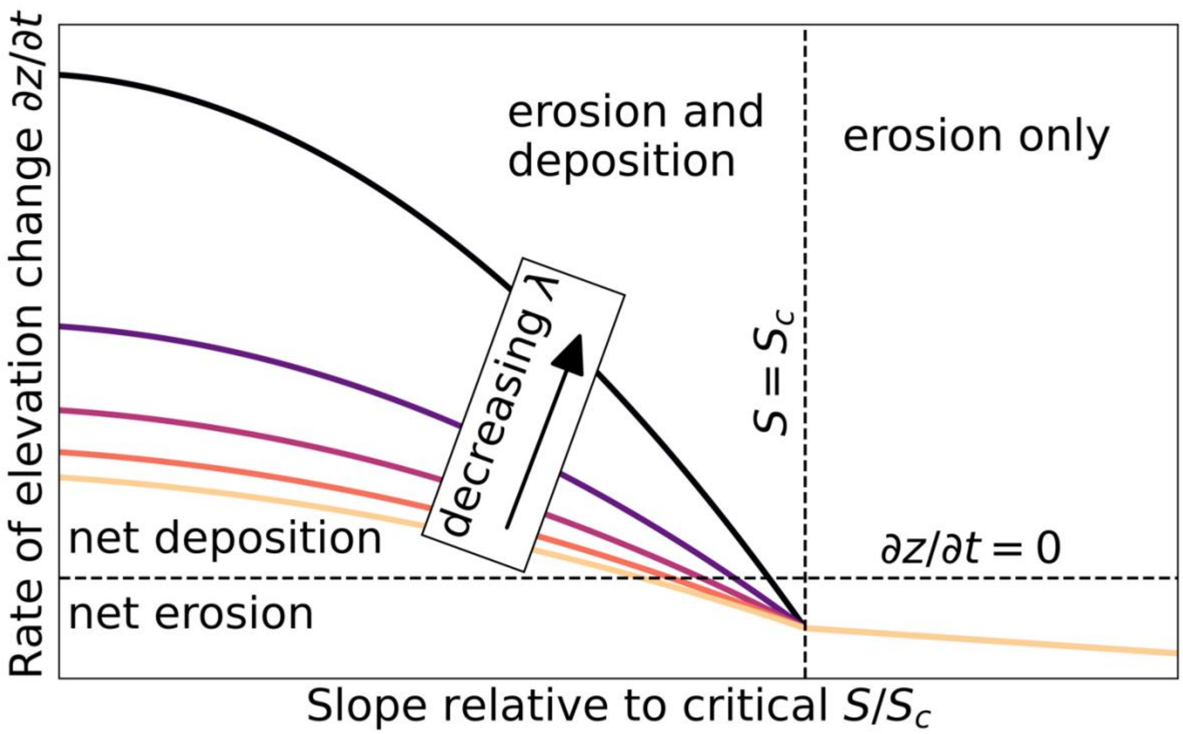


**Figure 1: Model behavior—as shown by the rate of elevation change—as a function of $\frac{S}{S_c}$ (where $S = \frac{\partial z}{\partial x}$) and $\lambda$. Decreasing the transport length scale leads to increased deposition, and therefore positive changes in elevation, when the slope is below the slope of non-deposition. When the slope is at or above the slope of non-deposition, the transport length scale ceases to matter because no deposition occurs and all sediment bypasses the cell. The sediment entrainment rate increases linearly with slope, and deposition rate decreases nonlinearly with slope, leading to net erosion as slopes increase towards the slope of non-deposition. The erosion coefficient is held constant in this figure.**

We follow previous work (Kaufman et al., 1992; van Balen et al., 1995) in our treatment of both the local, linear model and the nonlocal, nonlinear model by asserting that the erosion coefficient *K* declines exponentially with water depth (equation 3). This accounts for the erosive energy that may prevent the development of steep slopes close to the shoreline. The complete governing equation for the commonly used linear, local model in the erosion-deposition framework is found by substituting equations 3, 5, and 6 into equation 4, is therefore:

$$\frac{\partial z}{\partial t} = -K_0 e^{-d/d_*} \frac{\partial z}{\partial x} + \frac{q_s}{dx}. \quad (9)$$

The complete equation for bathymetric evolution under the nonlocal, nonlinear model is found by substituting equations 3, 5, and 8 into equation 4:

$$\frac{\partial z}{\partial t} = -K_0 e^{-d/d_*} \left|\frac{\partial z}{\partial x}\right| + \frac{q_s\left(1-\left(\left(\partial z/\partial x\right)/S_c\right)^2\right)}{\lambda}. \quad (10)$$

Equation 9 has two parameters: the sediment entrainment coefficient at zero water depth $K_0$ [L/T] and the depth scale $d_*$ [L] over which the entrainment coefficient declines with depth. Equation 10 has two additional parameters: the slope of non-deposition $S_c$ [-] and the sediment transport length scale $\lambda$ [L]. Sediment compaction due to the deposition of overburden is calculated using the assumption of an exponential decay in porosity $\varphi$ with depth below the bathymetric surface $h$ (e.g., Sclater and Christie, 1980; Yuan et al., 2019a):

$$\varphi(h) = \varphi_0 e^{-h/h_*}, \quad (11)$$

where $\varphi_0$ is the surface porosity and $h_*$ is the e-folding length scale governing the decay of porosity with depth.

**Conditions for the Collapse of the Nonlocal, Nonlinear Model to the Linear, Local Model**

The nonlocal, nonlinear model (equation 10) is convenient because it collapses to the common linear diffusion model (equation 9) under certain parameter values such that the key differences between the two approaches (the addition of a slope of non-deposition and a transport length scale) can be undone with parameter changes alone. When the slope of non-deposition $S_c$ is infinitely large, or in practice is many times greater than the greatest slopes in the model domain, there is no slope-driven reduction in the deposition rate and therefore no sediment bypass on steep slopes. Similarly, when the sediment transport length scale $\lambda$ is equal to the model grid spacing $dx$, there is no transport over flat regions. Parameter values in this model are therefore a direct proxy for model structure (e.g., Barnhart et al., 2020a), meaning that finding parameterizations that match observations can determine optimal model structure and yield insight into marine seascape evolution processes. This will allow us to test the applicability of both models to a stratigraphic dataset by asking whether best-fit model realizations exhibit parameter values that result in a collapse of the nonlocal, nonlinear model to the local, linear model.

## METHOD FOR INVERSION OF PASSIVE MARGIN STRATIGRAPHY

Our goal, rather than simulating margin evolution under an assumed set of parameter values, is to develop insight into model structure by using a data-driven inversion to find the set of parameter values that yields the best match between modeled and measured passive margin stratigraphy. Best-fit parameter values will illuminate whether the deviations from the linear diffusion approach encoded within our model (sediment bypass and long-distance transport) are necessary to match stratigraphic observations.

### Study Area: the Southeast Atlantic Margin, Southern Africa

The Southeast Atlantic Margin (SAM) is a well-studied passive margin sedimentary basin off the western coast of southern Namibia and South Africa (Figure 2). Our study area consists of the Cape, Orange, Lüderitz, and Walvis basins, which are bounded on the southeast by the Agulhas fracture zone and on the northwest by the Rio Grande fracture zone. The basins were initially formed by early Cretaceous rifting that opened the South Atlantic Ocean as Africa separated from South America (e.g., Hirsch et al., 2010). Rifting initiated at ca. 250 Ma (Hirsch et al., 2010), but we focus only on post-rift stratigraphy (Guillocheau et al., 2012; Baby et al., 2018; 2019). The earliest post-rift units are dated to ca. 131 Ma (Baby et al., 2019). The Orange River is the largest modern sediment source for the SAM; the thickest accumulations of sediment exist in the Orange Basin. We selected the SAM because of the large number of long (in terms of distance from the shoreline) seismic sections that have been collected and interpreted (Guillocheau et al., 2012; Baby et al., 2019). Sections that have continuous coverage from the shoreline to the nearly flat basin floor—typically reached at a distance of between 300 and 600 km from shore in the SAM—are essential to constraining the extent to which the long-distance sediment transport dynamics in our model adequately describe the development of passive margin stratigraphy.

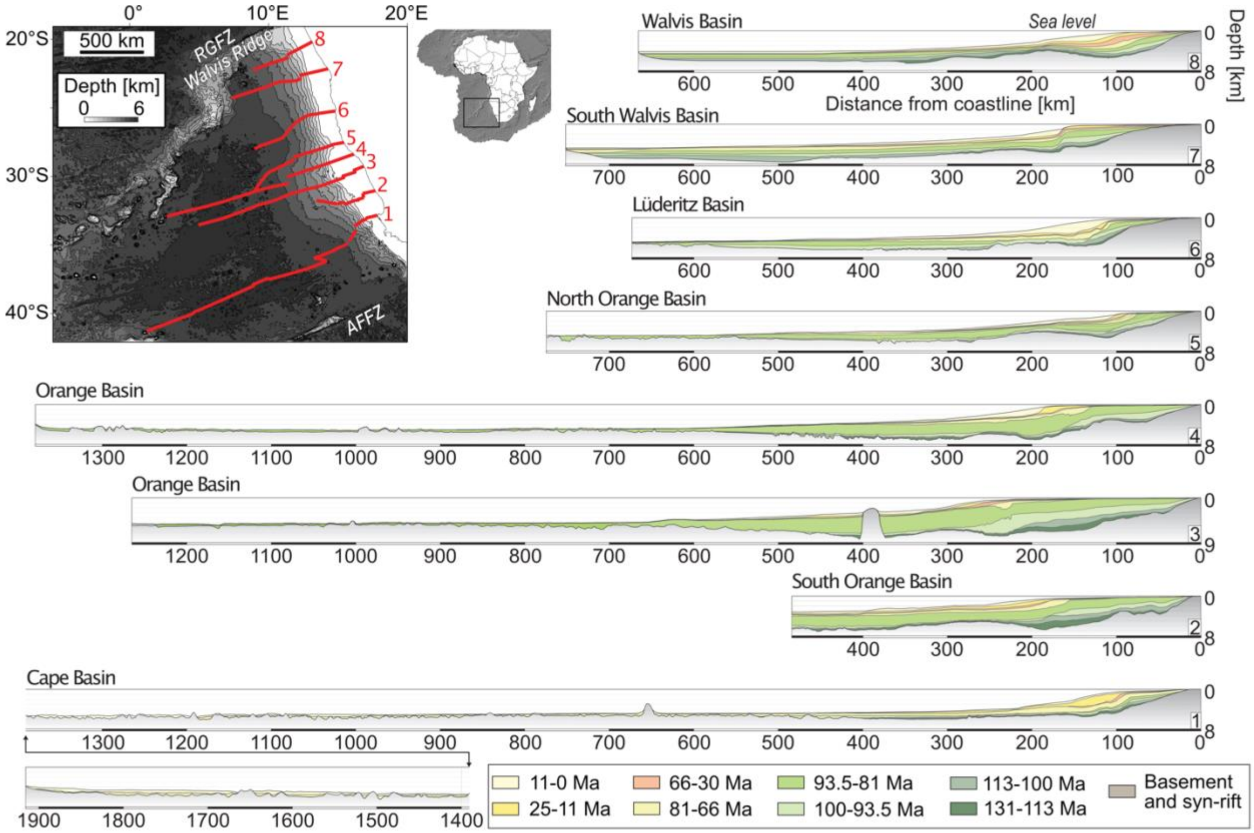


**Figure 2: Study area and seismic data, modified from Baby et al. (2019). We use sections 1 and 3-8 and retain the section numbers from Baby et al. (2019) for clarity. We do not use section 2 for our parameter estimation experiments because it is too short; the thickness of deposits beyond 500 km from the shoreline is unknown. RGFZ is the Rio Grande Fracture Zone; AFFZ is the Agulhas-Falkland Fracture Zone.**

Seven seismic sections interpreted by Baby et al. (2018; 2019) comprise the dataset that we will use to test the two models and determine optimal model structure and parameter values (Figure 2). We omit one of their sections—their section 2 (Figure 2)—from our analysis because it is by far the shortest section (< 500 km) and because at its end point there are deposits approximately 3 km thick. It is not possible to evaluate models for long-distance sediment transport using section 2 because the section ends before deposits reach a negligible thickness.

The data that is most easily compared to SFM output is the geometry of seismic reflectors. We use as our benchmark data sections that have been converted from two-way travel time to depth. Each section has nine seismic reflectors of interest, each representing the top of a particular unit as defined by Baby et al. (2019). The first (deepest) reflector of interest is the contact between basement/syn-rift deposits and the first post-rift deposits, interpreted by Baby et al. (2019) to occur at ca. 131 Ma. The ninth (uppermost) reflector is the modern bathymetric surface. Because the basement/syn-rift surface will be manipulated as a model boundary condition, there remain eight reflectors that could potentially be used for model-data comparison when determining best-fit model structure and parameter values.

**Inversion Methodology**

The general procedure of our data-driven inversion approach—more formally classified as a parameter inference exercise—is to run successive "generations" (sets of realizations) of the model that are run in parallel and then compared against data using a misfit function we define. The first generation uses parameter values randomly drawn from a uniform distribution. Each generation yields a subset of model runs with acceptable fits; a new generation of model realizations is then created by randomly perturbing the parameter values of the runs from the previous generation that were deemed acceptable. By running successive generations of realizations, the inversion procedure converges on a region of the parameter space that yields the best-fitting parameter values. Because model parameter values represent the contributions of slope bypass and long-distance transport processes, best-fit parameter values reveal the importance of those processes to passive margin evolution. For our inversions we used the ABC-SMC (approximate Bayesian computation—sequential Monte Carlo) algorithm implemented in PyABC (Klinger et al., 2018), an open-source Python package that allows efficient parameter estimation using the iterative procedure described above. See Sisson et al. (2007) and Toni et al. (2009) for details of ABC-SMC approaches. See Table S1 for algorithm parameters used in our study.

Conducting such an inversion exercise requires estimating or assuming initial and boundary conditions for the numerical model that cannot be precisely known from the geophysical and stratigraphic data (for example, the subsidence history of the basin floor over the past 130 Ma). We also need to define how model-data misfit will be calculated.

***Initial and Boundary Conditions***

Because our goal is to invert for best-fit model parameters, rather than boundary conditions, we must assume a set of boundary conditions lest we introduce too many variables into the inversion. The two key boundary conditions, both of which are functions of time, are the geometry of the basement/syn-rift layer and the sediment flux to the modeled basin.

***Basement geometry.*** We set initial basement geometry at 130 Ma by assuming that the initial post-rift basement had approximately 1/3 the depth, relative to a steady datum, of the modern basement. We then assumed that the basement subsided at an exponentially declining rate (McKenzie, 1978) between 130 Ma and present, such that the basement elevation over time at any point declines from its initial elevation to its known present elevation, rapidly at first and then more slowly (with an e-folding time scale held constant at 23.67 Ma for all sections). These simplistic assumptions are broadly consistent with expectations derived from simple thermal subsidence models (e.g., McKenzie, 1978) and gives time series of basement elevations in agreement with those deduced from basin reconstruction studies from the Orange Basin (Hirsch et al., 2010).

The key simplification inherent to our treatment of basement geometry is that we do not include any uplift or tilting of the margin over the course of its evolution. Stratigraphic analysis (Baby et al., 2018), thermochronologic measurements (Stanley et al., 2021), basin modeling (Hirsch et al., 2010), and numerical modeling (Dauteuil et al., 2013; Braun et al., 2014; Stanley et al., 2021) suggest that portions of the SAM experienced two periods of rock uplift. The first is a pulse of tilting from ca. 81-66 Ma that affected the Orange and Lüderitz basins and could have caused a maximum of 1,000 m of rock uplift in the proximal portion of the margin (the distal portions of the margin, closer to the hinge point of the tilt, would have experienced much less rock uplift; Aizawa et al., 2000; Paton et al., 2008; Hirsch et al., 2010; Baby et al., 2018). This pulse is hypothesized to result from passage of Southern Africa over a mantle superswell (Braun et al., 2014). The second hypothesized rock uplift pulse occurred at ca. 30 Ma (though basin reconstruction studies report the pulse as occurring later at ca. 16 Ma (Hirsch et al., 2010)) and had an amplitude of approximately 300-350 m (Baby et al., 2018); the cause of this pulse remains unknown. We choose not to incorporate these perturbations into our basement boundary condition. The magnitude and timing of uplift pulses are inconsistent—and inconsistently constrained—among the four basins for which we have data (Baby et al., 2018), and there is still debate about the existence and importance of the more recent proposed pulse (Mallard and Salles, 2021; O'Malley et al., 2021). The magnitude of these perturbations is small relative to the up to 7 km of deposits on the SAM. We acknowledge that incorporating these uplift pulses might improve model-data misfit, but we argue that there is insufficient clarity in the data to incorporate them, and that neglecting them would not lead to different conclusions with respect to differentiating between the models being investigated here.

***Terrestrial sediment flux.*** Basin-scale sediment flux reconstructions for the SAM rely on interpolation between seismic sections to derive estimates of volumetric sediment delivery to the margin over the past 130 Ma (Guillocheau et al., 2012; Baby et al., 2019). However, a cursory look at the sections of interest (Figure 2) shows that the total sediment volume, as well as the volume during any given time interval, varies significantly among sections within a given basin.

To remove any potential uncertainty surrounding the role of sediment flux, we take the simplest possible approach: for each stratigraphic section to which we compare our model, we calculate the sediment flux for each time period by integrating for the volume of sediment per unit margin width contained between each set of reflectors along each section while accounting for post-deposition porosity loss due to compaction (see supplemental section S1; Sclater and Christie, 1980; Allen and Allen, 2013). This approach yields a total sediment volume per unit basin width [$L^2$] for each unit in each section. Because the time duration represented by each section is known from previous work (Guillocheau et al., 2012; Baby et al., 2019), we can then divide each unit's volume per unit basin width by the time interval to get an average sediment flux to the section per unit time [$L^2/T$]. Figure 3 shows the sediment flux time series obtained by integration, as well as the basin-integrated sediment flux time series from Baby et al. (2019). The sediment flux time series in any one section is reasonably similar to the basin-integrated sediment flux. Estimates from our section integration approach are subject to uncertainty due to stratigraphic incompleteness (e.g., Straub et al., 2020) caused by sediment moving into and out of the plane of the section (i.e., parallel to the margin). Given that the alternative is to assume that reconstructed basin-scale sediment fluxes were evenly distributed among all sections in a given basin, an idea not supported by section volumes or isopach maps (Baby et al., 2019), we argue that we have made the safer assumption by conserving mass within each section we analyze.

***Sea level.*** We hold sea level constant throughout all model experiments. The amplitude of eustatic sea level variations (~120 m) is small relative to the length and depth scales of the SAM both globally over the past 100 Ma (Bessin et al., 2017) and more recently throughout the Quaternary off southern Africa specifically (Ramsay and Cooper, 2002).

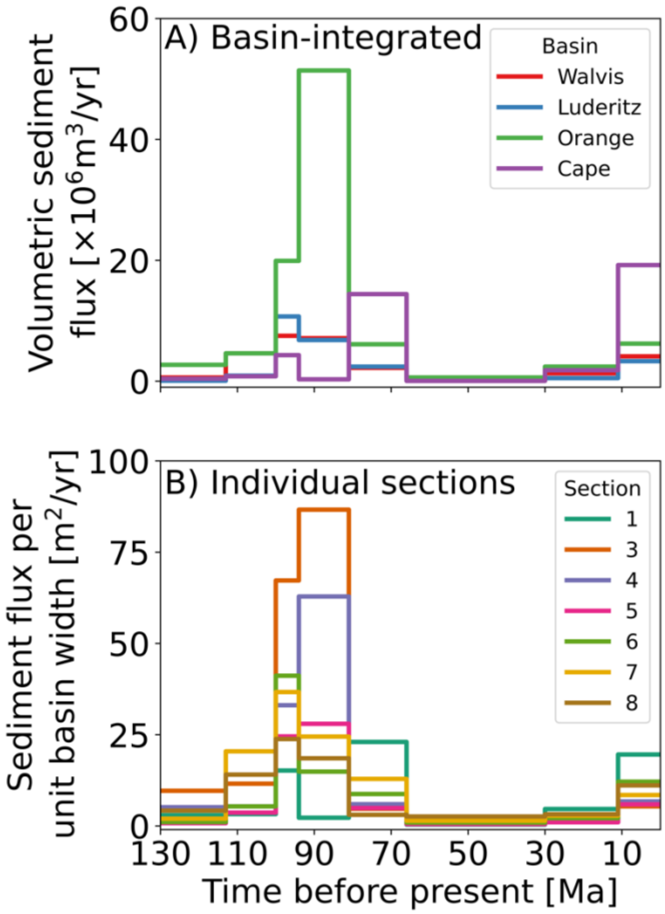


**Figure 3: (A) Volumetric fluxes of solid sediment from southern Africa to the four basins comprising the SAM (Baby et al., 2019). These estimates were derived from interpolating between the sections shown in Figure 3 (Guillocheau et al., 2012; Baby et al., 2019). (B) Volumetric solid sediment fluxes per unit basin width derived in this study by integrating over the depth and length of each seismic section and assuming an exponentially declining porosity profile. The latter method ensures that the amount of mass being delivered to the basin during a model realization is consistent with that observed in the section, such that sediment flux variability is removed as a potential control on model-data fit. Given that the basins range from 500-1000 km wide, the two estimates agree to an order of magnitude.**

### ***Inversion Experimental Setup***

Given the data available for the SAM, there are two potential ways to compare numerical model outcomes against the stratigraphic record. The first is to compare the modeled and measured modern bathymetric surface without taking into account the geometry of subsurface reflectors. This has the advantage of simplicity as it does not require calculations to account for the post-deposition compaction of older reflectors. The other potential avenue for comparison is to simultaneously compare between the model and the data the position of all reflectors (except for the top of the basement/syn-rift deposits, which is controlled by model boundary conditions). This latter approach is more complicated, but provides a time-integrated picture of model-data (mis)fit rather than relying on only the modern surface. The multi-reflector approach may be particularly important when working with data from the SAM, as the geometry of the uppermost layer (11-0 Ma) is thought to be heavily influenced by contour currents in addition to processes transporting sediment purely seaward from the coast (Baby et al., 2018).

We conduct two different inversion exercises: one that uses as a basis for model-data comparison only the modern bathymetric surface of the basin in each section (experiment 1), and one that uses the position of all reflectors simultaneously to assess model-data fit (experiment 2). In both analyses, best-fit model parameter values are constrained for each section independently. This approach allows us to then compare best-fit parameter values among sections to assess the variability of best-fit values across the SAM.

For each set of experiments, we also ran an inversion using a parameterization of our model that collapses to the standard linear diffusion model by setting the sediment transport length scale equal to the grid spacing and removing slope as a control on the sediment deposition rate. Comparison of best-fit results between the nonlocal, nonlinear model and the linear diffusion model will reveal whether the additional complexity we have implemented to approximate nonlocal, nonlinear sediment transport leads to model results that better match observations from the SAM.

***Experiment 1: Inversion using the modern bathymetric surface.*** In this experiment we compare the modeled bathymetric surface after 130 Ma to the bathymetric surface revealed in Baby et al. (2019). Because the basement elevation at 130 Ma of model time is imposed to match the observed basement elevation, this is equivalent to comparing the observed ($h_{obs}$) and modeled ($h_{sim}$) thickness of sediment deposited at every point *i* along the section. The misfit function can be written as:

$$\mu = \sqrt{\frac{1}{N-1}\sum_{i=1}^{N}\frac{(h_{obs}-h_{sim})^2}{\delta^2}}, (12)$$

where *N* is the number of cells in the model domain—and the number of points to which the seismic section has been downsampled—such that all points except for the boundary condition tied to $z = 0$ are considered. $\delta$ is the error associated with our observations. Because we do not have an explicit estimate of $\delta$ at every point, which would be a quantity derived during the seismic interpretation process, we choose to keep it constant at an arbitrary value of 10 m across all points of all sections. The value of $\delta$ has no influence on the inversion process because the divisor is constant throughout all of our experiments. Only in a case where one had reason to expect spatially or temporally varying $\delta$ would its value affect the search for a best-fit set of parameter values.

***Experiment 2: Inversion using all reflectors.*** Our second, more sophisticated inversion scheme compares the elevation above basement of the eight reflectors from a given seismic section against the same measurements from each modeled section. This comparison gives rise to the misfit function:

$$\mu = \sqrt{\frac{1}{N_r(N-1)}\sum_{j=1}^{N_r}\sum_{i=1}^{N}\frac{(h_{obs}-h_{sim})^2}{\delta^2}}, (13)$$

where $N_r$ is the number of reflectors being compared between each measured and modeled section (in our case $N_r = 8$).

## RESULTS AND DISCUSSION

### The Nonlocal, Nonlinear Model Calibrated Against the Modern Bathymetric Surface

***Best-fit Parameter Values***

Of the four parameters we varied in the nonlinear, nonlocal model, two dominate model behavior and show narrow ranges that yield the best fit to the stratigraphic data (Figure 4, Table S2). The two key parameters are the sediment transport distance and the slope of non-deposition. Inversions converge on relatively narrow best-fit regions for these two values, such that substantial deviation from the best-fit values results in much worse model-data fit. The same is not true of the surface sediment erodibility and the erodibility depth scale. For all seven sections, these parameters show large regions over which they provide fits of relatively unchanging quality. This indicates that the sediment transport distance and slope of non-deposition drive most of the variability in model outcomes. Physically, this suggests that it is the spatial pattern of deposition, rather than remobilization of previously deposited sediments, that shapes the SAM.

Comparing parameter distributions across the seven seismic sections (best seen in the kernel density plots in Figure 4) reveals that every section converges on best-fit parameters that depart significantly from the local, linear model. The majority of sections converge on values for the sediment transport length scale of slightly over $2\text{x}10^5$ m. Recalling that the local model is recovered with a value of $10^4$ m (the grid cell spacing for our experiments), this result indicates that the shape of the modern bathymetric surface in the SAM requires significant long-distance transport even across low slopes. The best-fit slope of non-deposition is between 0.02 and 0.05 for all sections except one—section 1—which has no portions of the parameter space that provide a good fit to the data (Figure 5). Such low slopes of non-deposition imply a significant role for slope bypass, or nonlocal downslope sediment transport. Best-fit $S_c$ values many times the maximum slopes observed on the SAM would indicate that sediment transport can be reasonably approximated by transport that depends only on local slope; we do not find support for this idea. Instead, the best fit between modeled and measured stratigraphy is achieved when sediment can bypass slopes of more than a few degrees.

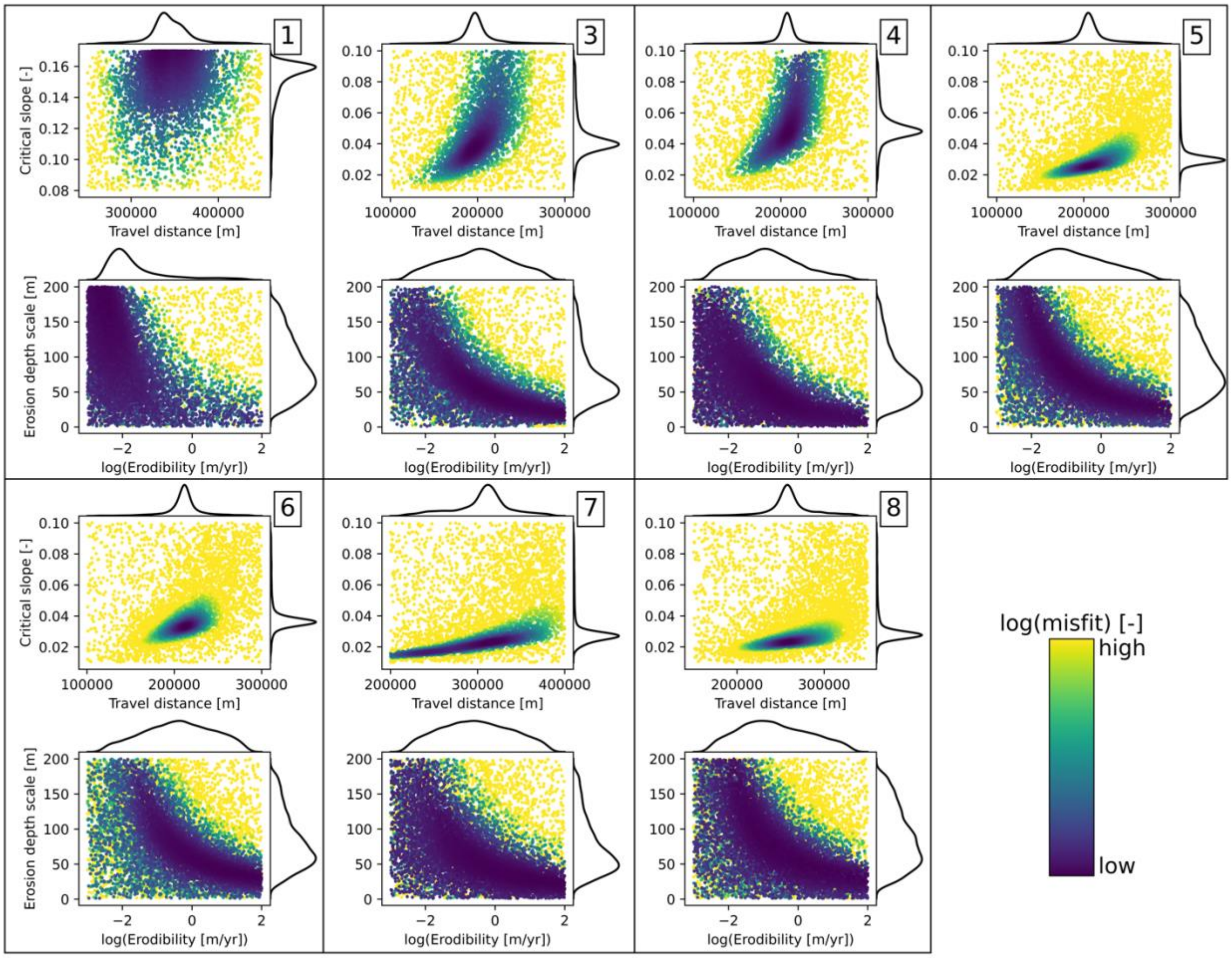


**Figure 4: Results for all seven sections from the search for a best-fit parameterization of the nonlocal, nonlinear model with the inversion procedure constrained only by the modern bathymetric surface. Scatter plots show model-data misfit (color) as a function of the four key parameters. Kernel density estimate (KDE) plots show the distribution of values for each parameter. Because the inversion procedure runs more model realizations in regions of the parameter space with reduced model-data misfit, peaks in the KDE plots can be interpreted as showing the region of each parameter's range that leads to the lowest misfit. Narrow peaks in the KDE plots indicate parameters with well-constrained best-fit values, while broad peaks indicate parameters for which a wide range of values produces similar misfit. Numbered sets of plots refer to the seismic section used for the inversion. Maximum and minimum misfit values vary between sections; color values have been scaled for maximum interpretability.**

### *Comparison of Modeled and Observed Stratigraphy*

For five of the seven sections, the inversion was able to yield best-fit parameter estimates that led to best-fit simulations that qualitatively and quantitatively fit the data reasonably well (Figure

5). These sections have gently sloping continental shelves with altitudes below, rather than level with, sea level, and smooth, convex-up shelf edges. They have concave-up continental slopes grading into gently sloping continental rise/abyssal plain deposits. Sediment is not always found as far from shore as in the data, but noticeable accumulations of sediment are observed up to ~1000 km from shore. Two sections, 1 and 7, yielded what we interpret to be substantially worse fits as defined by the mismatch of major morphometric features like the continental shelf edge and the curvature of the continental slope. It is difficult to be certain why the fits are substantially worse for sections 1 and 7. One key commonality that the two sections share is a relatively high proportion of the total sediment volume stored at the extreme distal end of the section. While our approach does allow for more realistic modeling of long-runout sediment transport than for example the classic linear diffusion approach, there is still a fundamental tension in which allowing sediment to accumulate at the very distal end of the modeled section requires too much inhibition of deposition at the proximal end. It may not be possible for our model to deposit enough sediment in distal reaches while preserving steep, well-defined shelf edges. This weakness would not be resolved in section 1 by raising the maximum possible $S_c$ value (Figure 4); increases in $S_c$ would further inhibit transport to the basin floor.

Comparison of modeled and observed subsurface reflectors, though it was not quantitatively incorporated into the misfit function in this experiment, shows that the pattern of reflectors is almost completely depositional. There are few—and only minor—instances of reflectors being truncated by overlying units, indicating that the story in these models is one of continuous deposition rather than episodes of deposition and re-erosion driven by variations in the terrestrial sediment flux time series. This is broadly concordant with the interpreted geologic history of the SAM, in which—barring the episodes of rock uplift that we have not modeled here—there is little erosional truncation of units except by eustatic variations in the nearshore. This concordance of modeled and observed stratigraphy suggests that our model is not only producing reasonable final bathymetry, but is building a stratigraphic record that reflects the long-term average of the processes shaping the SAM.

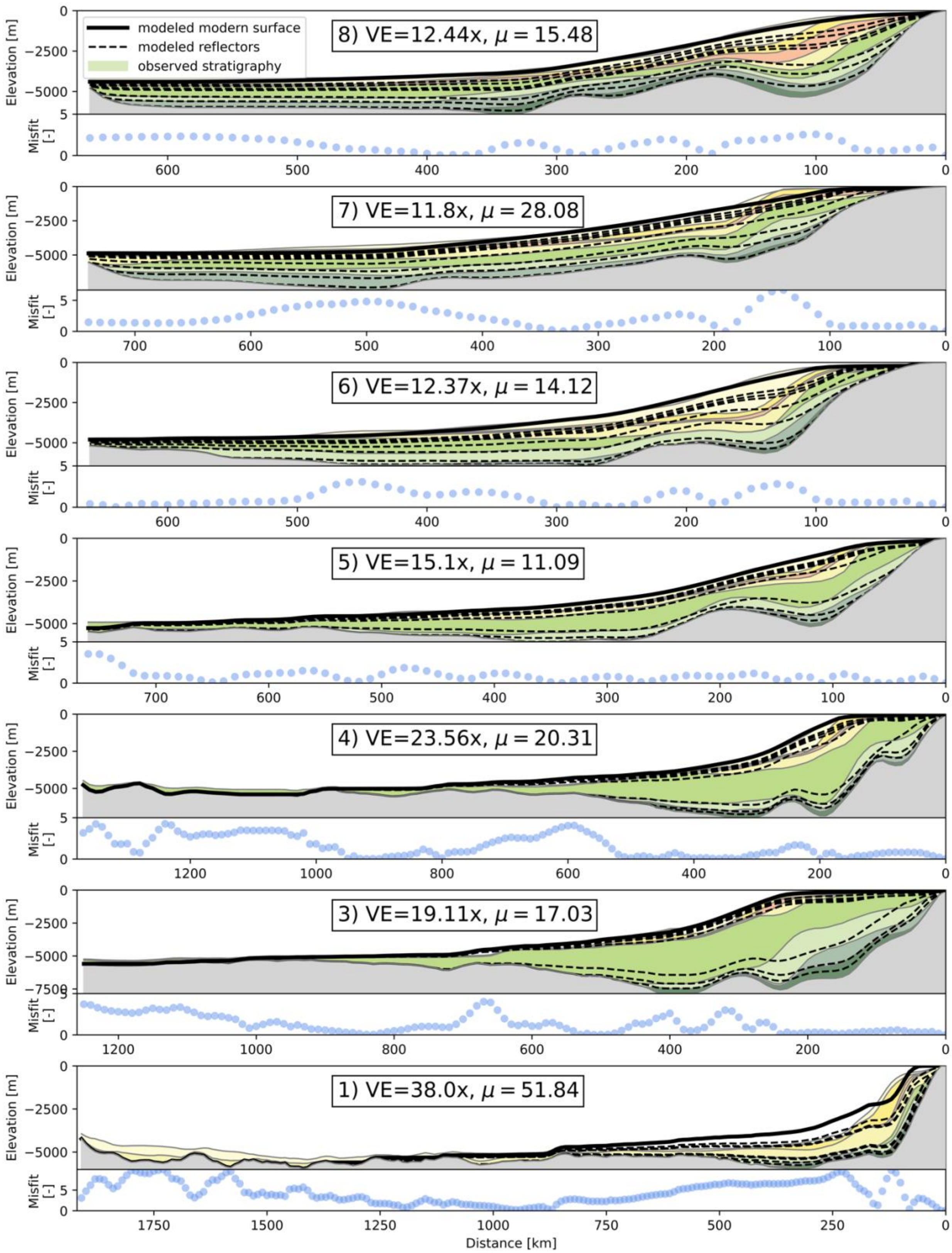


**Figure 5: Comparison between modeled and measured stratigraphy for all seven sections. While all modeled reflectors are shown (and are compacted to account for overburden), only the modern bathymetric surface**

**was used to assess model-data fit in this experiment; subsurface modeled reflectors were not compared against data to assess fit. Sections 3, 4, and 5 demonstrate cases in which the model yields both a low misfit as quantified by the difference between the measured and modeled modern bathymetric surface as well as reasonable modeled subsurface reflector positions. Section 1 in particular shows a case where the model was unable to find parameter values that yielded a good fit to the data. VE is vertical exaggeration.**

## Comparison Between the Nonlocal, Nonlinear Model and the Local, Linear Model

Here we compare inversion results between the two models to assess whether the nonlocal, nonlinear model leads to substantially better fits between modeled and measured stratigraphy. We search for the best-fit linear model using the same procedure as for our new model; the only two parameters to optimize in the linear model are the surface sediment erodibility $K$ and the depth scale over which it decays $d_*$.

Using only the modern bathymetric surface as a constraint, the local, linear model converges to a narrow range of surface erodibility values and a broader region of erodibility decay depths for section 3-8 (Figure 6, Table S2). Section 1, ever the outlier, converges on a large erodibility value that decays rapidly with depth. All sections except section 5 indicate that the model is "searching" for erodibility decay depth values even greater than the 40,000 m maximum value in the inversion. At the maximum values of 40,000 m, erodibility in the deepest parts of the margin only declines to ~80% of its value at the water surface such that sediment entrainment can still occur in the deep, distal reaches of the margin wherever nonzero slopes are found. Physically, we interpret this behavior as the local, linear model compensating for the lack of mechanisms for long-distance sediment transport by allowing substantial erosion at great depth. Interestingly, the tendency of the inversion procedure to identify $d_*$ values large enough that sediment erodibility does not meaningfully decline with depth suggests that while erodibility decay with depth may give rise to realistic-looking shallow marine morphometric features like shelf breaks (Kaufman et al., 1992; van Balen et al., 1995), such an approach may ultimately be counterproductive when we expand our view to include the distal portion of the margin because it yields models that cannot transport sediment far enough from shore without some additional component or further imposed changes in erodibility with depth or distance from shore.

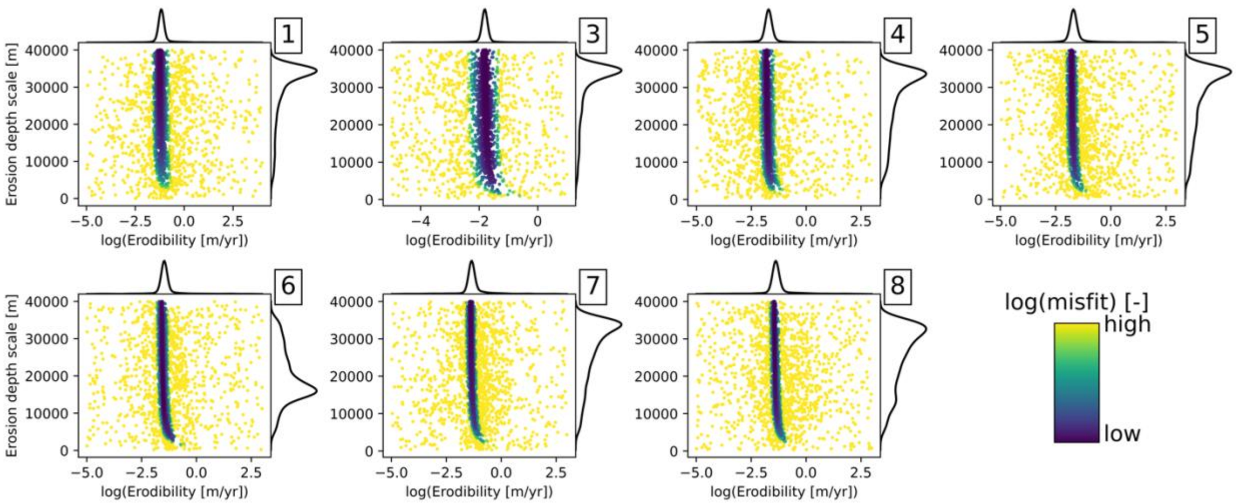


**Figure 6: Results for all seven sections from the search for best-fit parameter values for the local, linear diffusion model constrained only by the modern bathymetric surface. The tall, narrow region of good-fitting models indicates that a only narrow range of surface erodibility values leads to minimized misfit. The majority of sections (all except 6) have converged to the maximum values of the erodibility decay depth scale, indicating that even higher values would lead to further improvements in model-data fit. We imposed a maximum value of 40,000 m. Under these conditions, erodibility in the deepest regions of the margin only declines to approximately 80% of its value at the water surface. Further improvements to model-data fit from increasing the maximum decay depth would be marginal.**

The linear model provides, for all sections (3-7) that can be reasonably fit by either approach, a worse fit to the modern bathymetric surface than was obtained with the nonlocal, nonlinear model (Figure 7, 8). While best-fit parameterizations of the local, linear model do exhibit sediment delivery to the distal portions of the sections (achieved through large erodibility decay depths that yield non-negligible erodibility at depth), this comes at the cost of model-data fit in the nearshore environment. The large erodibility decay depths required to enable transport of sediment far from shore precludes the local, linear model from achieving the rounded, shallow continental shelf edge observed in the data. Instead, a shelf of sorts is created simply by progradation of the shoreline as sediments accumulate in the nearshore but are prevented by accumulating above sea level under the assumption that the shoreline will prograde under such conditions. Shoreline progradation, combined with an erodibility that is nearly constant throughout the depth profile, results in sharp shelf breaks grading immediately into the concave-up continental slope rather than the smooth, convex-up shelf breaks observed in the seismic data. The local, linear model is effectively being forced to choose between accurately reproducing the shelf edge and delivering sediment to the distal portions of the margin. Because our misfit function incorporates every point along each section, the model minimizes misfit if it delivers sediment far from shore even at the cost of reproducing the shelf and shelf-edge. A misfit function that focused on the nearshore (e.g., Yuan et al., 2019a) would likely lead to the opposite end-member of this tradeoff.

Though our misfit function in this experiment did not incorporate comparison between observed and modeled subsurface reflectors, the local, linear model—even in its best-fit parameterizations—does not stand up to a qualitative assessment of the form of the subsurface reflectors it produces (Figure 7). To deliver sediment far from shore, the local, linear model must first deposit that sediment in a proximal location and then erode those deposits during times of low terrestrial sediment flux. The time series of reflectors produced in most of the local, linear best-fit simulations reveals a steep, prograding wedge of sediment that is then smoothed out to lower gradients through a combination of subsequent erosion and truncation by overlying stratigraphic packages. Except for the brief periods in SAM history when the margin experienced substantial rock uplift, which we do not model, there is no evidence for significant erosional truncation beyond that occurring in the nearshore due to eustatic variations (Baby et al., 2019). The reflectors from the nonlocal, nonlinear model (Figure 5) do not show this pattern of progradation of a steep-fronted sediment wedge followed by later truncation by erosion; they instead show consistent accumulation of sediments through time at any given location, including the distal reaches of the basin. Interpretation of the stratigraphic record suggests that the latter behavior is more consistent with the history of the SAM.

It is unsurprising that the nonlocal, nonlinear model provides a better fit to the data than the local, linear model (Figure 8) in all but one case where neither model provided a reasonable fit and imposed parameter ranges prevented the more complex model from fully minimizing misfit (Figure 4)—the latter model is a restricted subset of the former. The critical results of this comparison are that (1) the model requires significant deviation from linear-diffusion parameter values (i.e., a large travel distance relative to the model grid cell spacing and a critical slope low enough that sediment bypass is common) to provide a reasonable match between modeled and observed bathymetry, (2) the local, linear diffusion model cannot through parameter adjustments provide fits that approximate—even to a less good-fitting degree—the outcomes of the nonlocal, nonlinear model, (3) the dynamics of the local, linear model as revealed by subsurface reflectors are not supported by observations from the SAM, and (4) seven of eight sections show a reduction in misfit—and four of seven sections show at least a factor of two reduction—achieved by adding nonlocal, nonlinear transport dynamics (Figure 8). This suggests that long-distance transport and slope-dependent sediment bypass processes are required to form the canonical shapes of passive margin stratigraphy, and therefore argues that these processes are essential ingredients in SFMs, at least for passive margin settings.

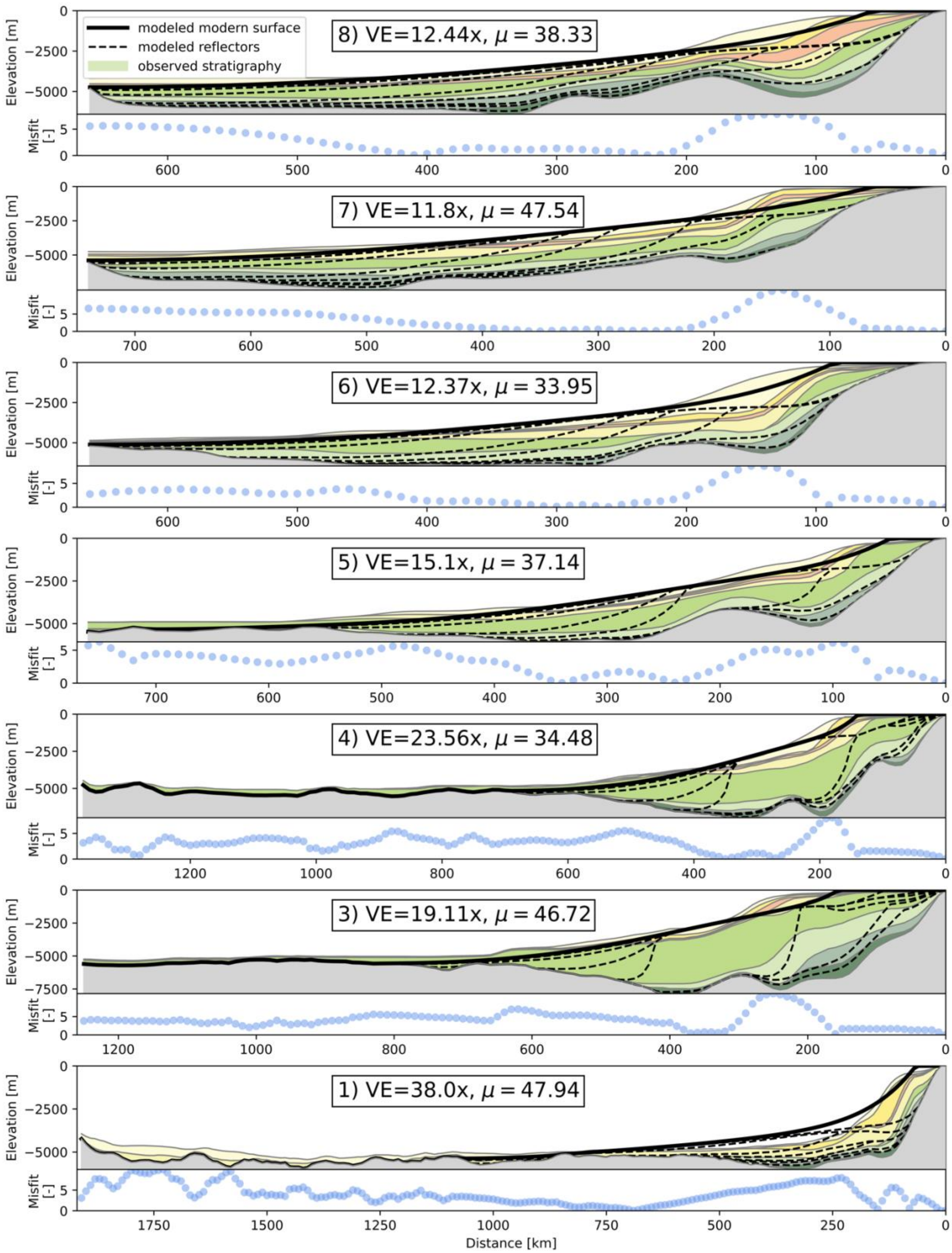

modeled modern surface
modeled reflectors
observed stratigraphy
8) VE=12.44x, $\mu = 38.33$
7) VE=11.8x, $\mu = 47.54$
6) VE=12.37x, $\mu = 33.95$
5) VE=15.1x, $\mu = 37.14$
4) VE=23.56x, $\mu = 34.48$
3) VE=19.11x, $\mu = 46.72$
1) VE=38.0x, $\mu = 47.94$
Elevation [m]
Misfit [-]
Distance [km]

**Figure 7: Comparison between modeled and measured stratigraphy for the best-fit local, linear diffusion model realization for each section. While all modeled reflectors are shown (and are compacted to account for overburden), only the modern bathymetric surface was used to assess model-data fit in this experiment; subsurface modeled reflectors were not compared against data to assess fit. Both the fit to the modern bathymetric surface and qualitative comparisons between modeled and observed subsurface reflectors reveal that the local, linear model cannot reproduce the geometry of the deposits observed in the SAM. The local, linear model exhibits significant truncation of lower units by upper units; such patterns are only observed in the SAM during times of rock uplift on the margin that we do not simulate in these experiments.**

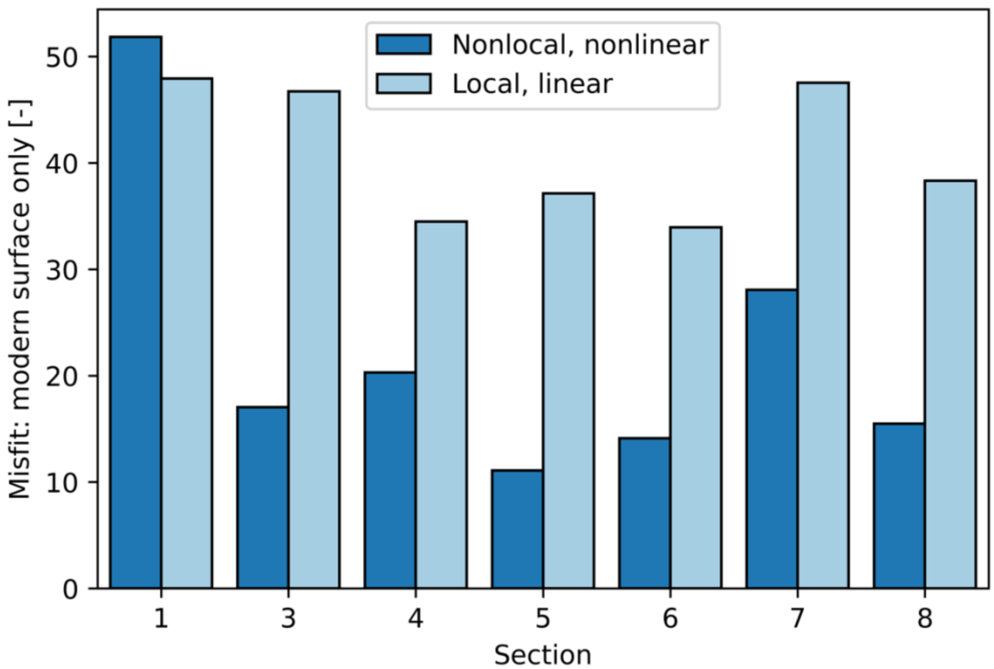


**Figure 8: Misfit values for the best-fit model for each section using the nonlocal, nonlinear model (dark blue) and the local, linear model (light blue) when the model fit is determined by comparing only against the modern bathymetric surface. The nonlocal, nonlinear model yields better fitting best-fit realizations for six of seven sections.**

## The Influence of Considering Multiple Reflectors

Parameters estimated by the inversion that takes into account all eight reflectors are surprisingly similar to those estimated when using only the modern bathymetric surface to constrain the inversion. For brevity we show average parameter values for the 50 best-fitting model realizations from the single reflector and multiple-reflector inversions plotted against each other (Figure 9) such that points falling on the 1:1 line indicate consistent parameter values achieved by the two methods. See Table S3 and Figures S1-S4 for detailed results of multi-reflector inversions.

Inclusion of all reflectors in the misfit calculation for the nonlocal, nonlinear model resulted in a shift towards slightly greater best-fit travel distance values (Figure 9A), likely because the data requires that good-fitting models be able to distribute sediment to the distal portion of the basin even relatively early in the margin's evolution when there do not yet exist the slopes required to drive sediment bypass in the absence of another mechanism for long-distance transport. The critical slope of non-deposition (Figure 9B) remained remarkably consistent between the surface-only and multiple-reflector inversions (), suggesting that the model most effectively adjusts to the need to deliver early deposits far from shore with changes in the travel distance, which affects transport over all slopes, rather than the critical slope, which only affects transport over meaningful bathymetric gradients. Physically, this may indicate the importance of long-runout sediment transport processes (e.g., turbidity currents, marine debris flows) that may initially be generated by significant bathymetric slopes but then transport sediment up to hundreds of km over vanishingly low slopes. The erodibility and erosion depth scale (Figure 9C and D, respectively) show more scatter between inversion methods; this is not surprising given that there is a large region of good-fitting values for both parameters as seen in the surface-only inversion (Figure 4).

Including all reflectors when searching for best-fit parameters for the local, linear model leads to surface erodibility values that largely fall near the 1:1 line (Figure 9E), indicating that the composition of the misfit function did not have a strong effect on the best-fit value. The same is true of the erodibility decay depth scale (Figure 9F) with the exception of two values that changed significantly between the surface-only and multiple-reflector inversion schemes. We attribute the overall consistency between parameter values derived using the two different methods to the fact that all reflectors in our seismic data show a similar pattern: long-distance transport beginning from the earliest stages of post-rift margin evolution followed by the largely depositional draping of successive units atop previous deposits. In this respect the modern surface is not geometrically distinct from the subsurface reflectors, which may explain why incorporating the subsurface reflectors leads to little improvement in model-data fit. A model can either achieve parameter values that allow it to develop these types of deposits (i.e., in the nonlocal, nonlinear model) in which case the specific number and age of reflectors used does not have a significant effect on inferred best-fit parameter values, or it cannot achieve parameterizations that allow long-distance, deposition-driven stratal stacking patterns (i.e., in the local, linear model) in which case the specifics of the misfit function do not matter because the fit to eight reflectors will be no better than the fit to a single one. We initially undertook the multiple-reflector inversion because the modern bathymetric surface is thought to be heavily influence by contour currents (Baby et al., 2018). Adding seven subsurface reflectors does not substantially change inferred best-fit parameters, which may indicate that variability in contour current effects among units does not cause a radical enough change in stratigraphic architecture—relative to the effects of subsidence and terrestrial sediment flux—to influence our relatively simple model.

When the misfit function incorporates all eight reflectors, the nonlocal, nonlinear model yields a better fit to the observed stratigraphic data than the local, linear model does for all seven sections (Figure 10). The improvement in model-data fit gained from adding nonlocal, nonlinear sediment transport dynamics exists regardless of whether we use only the modern surface or all reflectors as a basis for comparison. The misfit values between the two models are much closer when all reflectors were used for the inversion (Figure 10). This arises from the introduction of seven additional constraints on the model, many of which it must inevitably fail to match (Figure 5) even in its best-fit parameterization. However, the consistent reduction in misfit that accompanies the nonlocal, nonlinear model signals that those dynamics are required to produce stratigraphy that matches observations. The only scenario where this would not hold true is one in which a misfit function was used that did not take into account the distal portions of the basin at all. Given the substantial accumulations of sediment in the distal portions of the SAM (Figure 2), we argue that finding models that adequately simulate those deposits is a prerequisite for closing the source-to-sink mass balance.

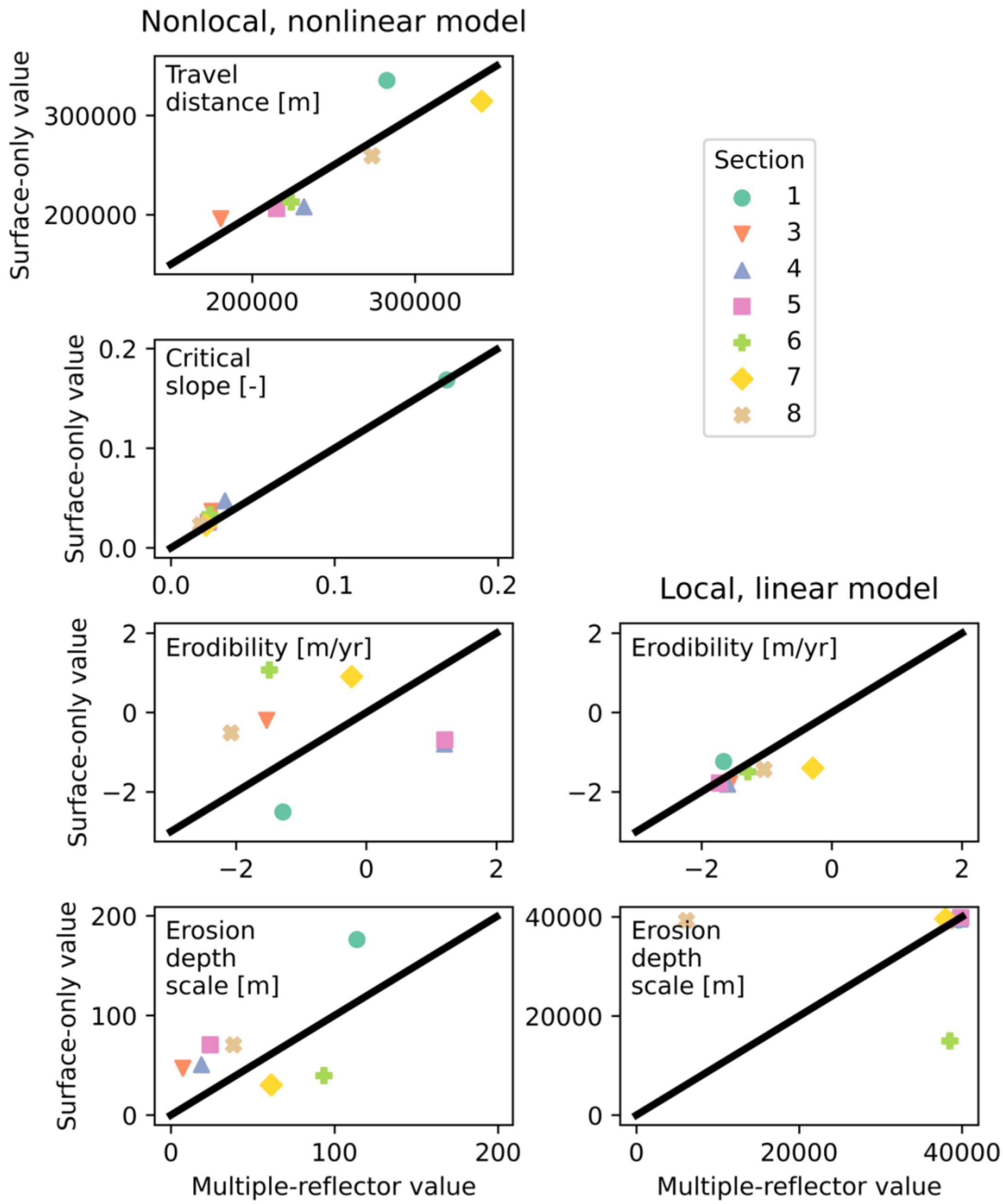


**Figure 9: Comparison between best-fit parameter values derived from the surface-only inversion and the multiple-reflector inversion. Black lines indicate a 1:1 match between parameter values derived by the two methods. In the case of the nonlinear, nonlocal model (column 1), the two most important parameters fall close to the 1:1 line, indicating that the inversion method (whether subsurface information is incorporated or not) does not have a strong influence on the best-fit parameter values and therefore on predicted margin stratigraphy. In the case of the local, linear model (column 2), erodibility values are consistent between methods while erosion depth scale values show more scatter.**

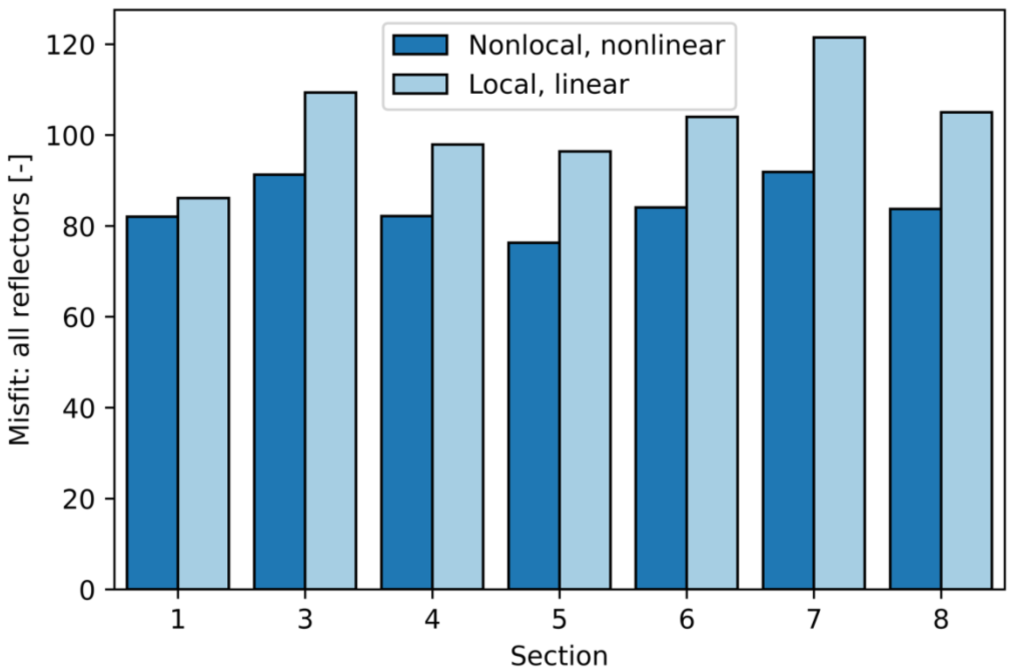


**Figure 10: Misfit values for the best-fit model for each section using the nonlocal, nonlinear model (dark blue) and the local, linear model (light blue) when the model fit is determined by comparing against all seismic reflectors. The nonlocal, nonlinear model yields better fitting best-fit realizations for all seven sections.**

## Limitations and Implications for Inversion of the Stratigraphic Record

Our motivation in testing SFMs is to enable the inversion of the stratigraphic record for information about past terrestrial environments and geomorphic processes. If reasonably effective SFM structures and parameterizations can be identified *a priori*, then coupled LEM/SFMs will be more useful for inferring for example tectonic or climatic perturbations to past landscapes. The SAM is already being used as a target for such studies (e.g., Mallard and Salles, 2021) due to its enigmatic climatic and tectonic history and its well-documented offshore stratigraphy. Though our study is confined to one passive margin, it strongly favors the idea that SFMs should incorporate mechanisms for sediment bypass and long-distance transport, and that these processes cannot be adequately mimicked with parameter changes in the commonly used local, linear diffusion model for seascape evolution.

The nonlocal, nonlinear model we tested represents an amalgamation of ideas from previous workers that had not been evaluated in detail against stratigraphic data, and our analysis reveals that it provides a substantial improvement over the more widely used local, linear model. However, the nonlocal, nonlinear model still needs improvement. Aside from subsuming a wide array of marine transport processes into two key transport parameters, its most critical shortcoming is that it only heuristically accounts for the momentum that allows transport processes like turbidity currents and marine debris flows to carry sediment into the distal portions of basins. More effective conceptualizations of sediment entrainment and disentrainment, possibly following recent advances in hillslope geomorphology (e.g., Doane et al., 2018; Furbish et al., 2021), might further improve SFMs with the understanding that the models will always need to simulate the spatial and temporal average of marine sediment transport if they are to prove feasible for inverse analyses that require $10^5$-$10^6$ forward model realizations. Improving model fit—especially abrupt slope breaks driven by changes in process dominance—may require multiprocess models (e.g., Granjeon et al., 1999; Syvitski and Hutton, 2001), but their parameter-rich nature may hinder parameter estimation exercises and make them susceptible to overfitting to a given calibration location. There exist sufficient models in the literature that span a wide range of complexity that, as in this study, the challenge is more about rigorously testing models against data to find the simplest workable theory than it is about developing new models.

Though we used eight seismic sections spanning four basins to evaluate different SFMs, our study is limited to a single passive margin. Best-fit regions of the parameter space for the nonlinear, nonlocal model's travel distance and critical slope of non-deposition parameters consistently showed that the model was not collapsing to its local, linear parameterization but likewise exhibited considerable variability among sections (Figure 4). While our analysis may have restricted the range of possible values that need to be considered when using such a model to invert the stratigraphic record, a set of “global” parameter values cannot be assumed. Tests against other stratigraphic datasets are needed to establish inter-basin, rather than intra-basin, variability in these key parameters. Alternatively, inversions could proceed by using model ensembles using a restricted subset of parameter values, which could still enable the removal of these parameters from the inversion and allow researchers to focus on extracting past forcings to source regions.

A final open question is that of model dimensionality. Our 1-D model enforces purely margin-perpendicular sediment transport, when in reality margin-parallel components of transport also occur. Though there exist plenty of 2-D SFMs (e.g., Granjeon and Joseph, 1999; Salles et al., 2018), testing optimal SFM structure in two dimensions remains an important stepping stone towards inverting terrestrial landscape history from stratigraphy.

## CONCLUSIONS

We introduced a simple, nonlocal, nonlinear model for marine sediment transport and the development of marine stratigraphy over geologic time. The model builds on the concepts of sediment bypass espoused by previous authors (e.g., Syvitski et al., 1998; Ross et al., 1994; Ding et al., 2019a; Mallard and Salles, 2021) that have not previously been directly tested against observed stratigraphy. Quantitative comparison of the model against seven stratigraphic sections from the SAM reveals that:

1. The nonlocal, nonlinear model can achieve parameterizations that develop realistic marine bathymetry and stratigraphy, though variability in best-fit parameter values exists among the seven seismic sections tested.
2. The nonlocal, nonlinear model does not converge on parameter values that result in a collapse to the commonly used local, linear model. The local, linear model cannot fit the data. It fails both to fit the modern bathymetric surface and to provide seascape evolution trajectories that match observations.
3. The key difference between the two models lies in the ability of the nonlocal, nonlinear model to deliver sediment to distal portions of the basin without compromising on the ability to develop realistic nearshore morphology and stratigraphy.
4. Points (1) through (3) hold true regardless of whether model parameters are optimized using only the modern bathymetric surface or the full suite of subsurface seismic reflectors, indicating that our results are robust to the specifics of the misfit function employed.
5. Processes of sediment bypass and long-distance transport govern the architecture of the stratigraphic record over basin-filling timescales, making it essential that SFMs capture at least the spatial and temporal averages of these nonlocal processes.

Given the general lack of terrestrial evidence for past landscape evolution dynamics, the stratigraphic record represents our best chance to learn about the erosion trajectories of landscapes long gone. We tentatively suggest that the transport dynamics encapsulated in the nonlocal, nonlinear model govern the development of passive margin stratigraphy. Our ability to invert the stratigraphic record, either on its own for inferring sediment supply to basins or coupled with landscape evolution models to infer past tectonic, climatic, and/or lithologic boundary conditions, would benefit from improved understanding of such nonlocal transport processes.

**ACKNOWLEDGMENTS**

Model code, data, and inversion scripts are publicly available at doi:[*repository to be made public upon acceptance*]. C.M. Shobe was supported by H2020 Marie Sklodowska-Curie Actions grant no. 833132 (STRATASCAPE). We acknowledge time on the West Virginia University Thorny Flat high-performance computing cluster which is supported by the National Science Foundation under Major Research Instrumentation program award #1726534. We thank Benoît Bovy, Tim Carr, Rachel Glade, Kim Huppert, Delphine Rouby, Jaime Toro, and Amy Weislogel for helpful discussions. Thanks to Guillermo Franco, Nate Garver-Daniels, and Daniel Turpen for HPC support.

**REFERENCES CITED**

Aizawa, M., Bluck, B., Cartwright, J., Milner, S., Swart, R., and Ward, J., 2000, Constraints on the geomorphological evolution of Namibia from the offshore stratigraphic record, Communications of the Geological Survey of Namibia, v. 12, p. 337—346.

Allen, P.A. and Allen, J.R., 2013, Basin Analysis, Principles and Application to Petroleum Play Assessment, Wiley-Blackwell, 632 p.

Andrews, D.J. and Bucknam, R.C., 1987, Fitting degradation of shoreline scarps by a nonlinear diffusion model, Journal of Geophysical Research: Solid Earth, v. 92, no. B12, p. 12857—12867, doi:10.1029/JB092iB12p12857.

Baby, G., Guillocheau, F., Morin, J., Ressouche, J., Robin, C., Broucke, O., and Dall'Asta, M., 2018, Post-rift stratigraphic evolution of the Atlantic margin of Namibia and South Africa: Implications for the vertical movements of the margin and the uplift history of the South African Plateau, Marine and Petroleum Geology, v. 97, p. 169—191, doi:10.1016/j.marpetgeo.2018.06.030.

Baby, G., Guillocheau, F., Braun, J., Robin, C., and Dall'Asta, M., 2019, Solid sedimentation rates history of the Southern African continental margins: Implications for the uplift history of the South African Plateau, Terra Nova, v. 32, no. 1, p. 53—65, doi:10.1111/ter.12435.

van Balen, R.T., van der Beek, P.A., and Cloetingh, S.A.P.L., 1995, The effect of rift shoulder erosion on stratal patterns at passive margins: Implications for sequence stratigraphy, Earth and Planetary Science Letters, v. 134, p. 527—544, doi:10.1016/0012-821X(95)98955-L.

Barnhart, K.R., Glade, R.C., Shobe, C.M., and Tucker, G.E., 2019, Terrainbento 1.0: a Python package for multi-model analysis in long-term drainage basin evolution, Geoscientific Model Development, v. 12, p. 1267—1297, doi:10.5194/gmd-12-1267-2019.

Barnhart, K.R., Tucker, G.E., Doty, S., Shobe, C.M., Glade, R.C., Rossi, M.W., and Hill, M.C., 2020a, Inverting topography for landscape evolution model process representation: Part 1, conceptualization and sensitivity analysis, Journal of Geophysical Research: Earth Surface, v. 125, no. 7, doi:10.1029/2018JF004961.

Barnhart, K.R., Tucker, G.E., Doty, S., Shobe, C.M., Glade, R.C., Rossi, M.W., and Hill, M.C., 2020b, Inverting topography for landscape evolution model process representation: Part 2, calibration and validation, Journal of Geophysical Research: Earth Surface, v. 125, no. 7, doi:10.1029/2018JF004963.

Barnhart, K.R., Tucker, G.E., Doty, S., Shobe, C.M., Glade, R.C., Rossi, M.W., and Hill, M.C., 2020c, Inverting topography for landscape evolution model process representation: Part 3, determining parameter ranges for select mature geomorphic transport laws and connecting changes in fluvial erodibility to changes in climate, Journal of Geophysical Research: Earth Surface, v. 125, no. 7, doi:10.1029/2019JF005287.

Beaumont, C., Fullsack, P., and Hamilton, J., 1992, Erosional control of active compressional orogens, *in* McClay, K.R., ed., Thrust tectonics, p. 1—18.

van der Beek, P., and Bishop, P., 2003, Cenozoic river profile development in the Upper Lachlan catchment (SE Australia) as a test of quantitative fluvial incision models, Journal of Geophysical Research: Solid Earth, v. 108, no. B6, doi:10.1029/2002JB002125.

Bessin, P., Guillocheau, F., Robin, C., Braun, J., Bauer, H., and Schroëtter, J.-M., 2017, Quantification of vertical movement of low elevation topography combining a new compilation of global sea-level curves and scattered marine deposits (Armorican Massif, western France), Earth and Planetary Science Letters, v. 470, p. 25—36, doi:10.1016/j.epsl.2017.04.018.

Bornholdt, S., Nordlund, U., and Westphal, H., 1999, Inverse stratigraphic modeling using genetic algorithms, *in:* Harbaugh, J.W., Watney, W.L., Rankey, E.C., Slingerland, R., Goldstein, R.H., and Franseen, E.K., eds., Numerical Experiments in Stratigraphy: Recent Advances in Stratigraphic and Sedimentologic Computer Simulations, doi:10.2110/pec.99.62.0085.

Braun, J., 2021, Comparing the transport-limited and $\zeta$-q models for sediment transport, Earth Surface Dynamics Discussions, doi:10.5194/esurf-2021-76.

Braun, J., Deschamps, F., Rouby, D., and Dauteuil, O., 2013, Flexure of the lithosphere and the geodynamical evolution of non-cylindrical rifted passive margins: Results from a numerical model incorporating variable elastic thickness, surface processes and 3D thermal subsidence, Tectonophysics, v. 604, p. 72—82, doi:10.1016/j.tecto.2012.09.033.

Braun, J., Guillocheau, F., Robin, C., Baby, G., and Jelsma, H., 2014, Rapid erosion of the Southern African Plateau as it climbs over a mantle superswell, Journal of Geophysical Research: Solid Earth, v. 119, p. 6093—6112, doi:10.1002/2014JB010998.

Burgess, P.M., Lammers, H., van Oosterhout, C., and Granjeon, D., 2006, Multivariate sequence stratigraphy: Tackling complexity and uncertainty with stratigraphic forward modeling, multiple scenarios, and conditional frequency maps, American Association of Petroleum Geologists Bulletin, v. 90, no. 12, p. 1883—1901, doi:10.1306/06260605081.

Campforts, B., Shobe, C.M., Steer, P., Vanmaercke, M., Lague, D., and Braun, J., 2020, HyLands 1.0: a Hybrid Landscape evolution model to simulate the impact of landslides and landslide-derived sediment on landscape evolution, v. 13., p. 3863—3886, doi:10.5194/gmd-13-3863-2020.

Carretier, S., Martinod, P., Reich, M., and Godderis, Y., 2016, Modelling sediment clasts transport during landscape evolution, Earth Surface Dynamics, v. 4, p. 237—251, doi:10.5194/esurf-4-237-2016.

Cross, T.A. and Lessenger, M.A., 1999, Construction and application of a stratigraphic inverse model, *in:* Harbaugh, J.W., Watney, W.L., Rankey, E.C., Slingerland, R., Goldstein, R.H., and Franseen, E.K., eds., Numerical Experiments in Stratigraphy: Recent Advances in Stratigraphic and Sedimentologic Computer Simulations, doi:10.2110/pec.99.62.0069.

Dauteuil, O., Rouby, D., Braun, J., Guillocheau, F., and Deschamps, F., 2013, Post-breakup evolution of the Namibian margin: Constrains from numerical modeling, Tectonophysics, v. 604, p. 122—138, doi:10.1016/j.tecto.2013.03.034.

Davy, P. and Lague, D., 2009, Fluvial erosion/transport equation of landscape evolution models revisited, Journal of Geophysical Research, v. 114, F03007, doi:10.1029/2008JF001146.

DiBiase, R.A. and Whipple, K.X., 2011, The influence of erosion thresholds and runoff variability on the relationships among topography, climate, and erosion rate, Journal of Geophysical Research, v. 116, doi:10.1029/2011JF002095.

Ding, X., Salles, T., Flament, N., Mallard, C., and Rey, P.F., 2019a, Drainage and sedimentary responses to dynamic topography, Geophysical Research Letters, v. 46, no. 24, p. 14385—14394, doi:10.1029/2019GL084400.

Ding, X., Salles, T., Flament, N., and Rey, P., 2019b, Quantitative stratigraphic analysis in a source-to-sink numerical framework, Geoscientific Model Development, v. 12, p. 2571—2585, doi:10.5194/gmd-12-2571-2019.

Doane, T.H., Furbish, D.J., Roering, J.J., Schumer, R., and Morgan, D.J., 2018, Nonlocal sediment transport on steep lateral moraines, Eastern Sierra Nevada, California, USA, Journal of Geophysical Research: Earth Surface, v. 123, no. 1, p. 187—208, doi:10.1002/2017JF004325.

Foufoula-Georgiou, E., Ganti, V., and Dietrich, W.E., 2010, A nonlocal theory of sediment transport on hillslopes, Journal of Geophysical Research: Earth Surface, v. 115, no. F2, doi:10.1029/2009JF001280.

Furbish, D.J. and Roering, J.J., 2013, Sediment disentrainment and the concept of local versus nonlocal transport on hillslopes, Journal of Geophysical Research: Earth Surface, v. 118, no. 2, p. 937—952, doi:10.1002/jgrf.20071.

Furbish, D.J., Roering, J.J., Doane, T.H., Roth, D.L., Williams, S.G., and Abbott, A.M., 2021, Rarefied particle motions on hillslopes—Part 1: Theory, Earth Surface Dynamics, v. 9, np. 3, p. 539—576, doi:10.5194/esurf-9-539-2021.

Granjeon, D. and Joseph, P., 1999, Concepts and applications of a 3-D multiple lithology, diffusive model in stratigraphic modeling, *in:* Harbaugh, J.W., Watney, W.L., Rankey, E.C., Slingerland, R., Goldstein, R.H., and Franseen, E.K., eds., Numerical Experiments in Stratigraphy: Recent Advances in Stratigraphic and Sedimentologic Computer Simulations, p. 197—210, doi:10.2110/pec.99.62.0197..

Guerit, L., Yuan, X.P., Carretier, S., Bonnet, S., Rohais, S., Braun, J., and Rouby, D., 2019, Fluvial landscape evolution controlled by the sediment deposition coefficient: Estimation from experimental and natural landscapes, Geology, v. 47, no. 9, p. 853—856, doi:10.1130/G46356.1.

Guillocheau, F., Rouby, D., Robin, C., Helm, C., Rolland, N., Le Carlier de Veslud, C., and Braun, J., 2012, Quantification and causes of the terrigeneous sediment budget at the scale of a continental margin: a new method applied to the Namibia-South Africa margin, Basin Research, v. 24, p. 3—30, doi:10.1111/j.1365-2117.2011.00511.x.

Hereema, C.J. et al., 2020, What determines the downstream evolution of turbidity currents? Earth and Planetary Science Letters, v. 532, doi:10.1016/j.epsl.2019.116023.

Hirsch, K.K., Schenck-Wenderoth, M., van Wees, J.-D., Kuhlmann, G., and Paton, D.A., 2010, Tectonic subsidence history and thermal evolution of the Orange Basin, Marine and Petroleum Geology, v. 27, p. 565—584, doi:10.1016/j.marpetgeo.2009.06.009.

Hobley, D.E.J., Sinclair, H.D., Mudd, S.M., and Cowie, P.A., 2011, Field calibration of sediment flux dependent river incision, Journal of Geophysical Research: Earth Surface, v. 116, no. F4, doi:10.1029/2010JF001935.

Jerolmack, D.J. and Paola, C., 2010, Shredding of environmental signals by sediment transport, Geophysical Research Letters, v. 37, no. 19, doi:10.1029/2010GL044638.

Kaufman, P., Grotzinger, J.P., and McCormick, D.S., 1992, Depth-dependent diffusion algorithm for simulation of sedimentation in shallow marine depositional systems, Kansas Geological Survey Bulletin, v. 233, p. 489—508.

Kenyon, P.M. and Turcotte, D.L., 1985, Morphology of a delta prograding by bulk sediment transport, Geological Society of America Bulletin, v. 96, no. 11, p. 1457—1465, doi:10.1130/0016-7606(1985)96<1457:MOADPB>2.0.CO;2.

Klinger, E., Rickert, D., and Hasenauer, J., 2018, pyABC: distributed, likelihood-free inference, Bioinformatics, v. 34, no. 20, p. 3591—3593, doi:10.1093/bioinformatics/bty361.

Kooi, H. and Beaumont, C., 1994, Escarpment evolution on high-elevation rifted margins: Insights derived from a surface processes model that combines diffusion, advection, and reaction, Journal of Geophysical Research, v. 99, no. 12, p. 12191—12209.

Lessenger, M.A. and Cross, T.A., 1996, An inverse stratigraphic simulation model—is stratigraphic inversion possible? Energy Exploration and Exploitation, v. 14, no. 6, p. 627—637, doi:10.1177/014459879601400606.

Lowe, D.R., Grain flow and grain flow deposits, *Journal of Sedimentary Petrology*, v. 46, no. 1, p. 188—199.

Luchi, R., Balachandar, S., Seminara, G., and Parker, G., 2018, Turbidity currents with equilibrium basal driving layers: A mechanism for long runout, Geophysical Research Letters, v. 45, no. 3, p. 1518—1526, doi:10.1002/2017GL075608.

Mallard, C.A. and Salles, T., 2021, Landscape responses to dynamic topography and climate change on the South African source-to-sink system since the Oligocene, *Earth Surface Dynamics Discussions*, doi:10.5194/esurf-2021-89.

McKenzie, D., 1978, Some remarks on the development of sedimentary basins, Earth and Planetary Science Letters, v. 40, no. 1, p. 25—32, doi:10.1016/0012-821X(78)90071-7.

Mohrig, D., Ellis, C., Parker, G., Whipple, K.X., and Hondzo, M., 1998, Hydroplaning of subaqueous debris flows, Geological Society of America Bulletin, v. 110, no. 3, p. 387—394, doi:10.1130/0016-7606(1998)110<0387:HOSDF>2.3.CO;2.

Molnar, P., Brown, E.T., Burchfiel, B.C., Deng, Q., Feng, X., Li, J., Raisbeck, G.M., Shi, J., Zhangming, W., Yiou, F., and You, H., 1994, Quaternary climate change and the formation of river terraces across growing anticlines on the north flank of the Tien Shan, China, The Journal of Geology, v. 102, no. 5, p. 583—602, doi:10.1086/629700.

Moretti, I. and Turcotte, D.L., 1985, A model for erosion, sedimentation, and flexure with application to New Caledonia, Journal of Geodynamics, v. 3, no. 1—2, p. 155—168, doi:10.1016/0264-3707(85)90026-2.

O'Malley, C.P.B., White, N.J., Stephenson, S.N., and Roberts, G.G., 2021, Large-scale tectonic forcing of the African Landscape, Journal of Geophysical Research: Earth Surface, v. 126, doi:10.1029/2021JF006345.

Niedoroda, A.W., Reed, C.W., Swift, D.J.P., Arato, H., and Hoyanagi, K., 1995, Modeling shore-normal large-scale coastal evolution, Marine Geology, v. 126, p. 181—199, doi:10.1016/0025-3227(95)98961-7.

Paola, C., 2000, Quantitative models of sedimentary basin filling, Sedimentology, v. 47, no. s1, p. 121—178, doi:10.1046/j.1365-3091.2000.00006.x.

Parker, G., Fukushima, Y., and Pantin, H.M., 1986, Self-accelerating turbidity currents, Journal of Fluid Mechanics, v. 171, p. 145—181, doi:10.1017/S0022112086001404.

Paton, D.A., van der Spuy, D., di Primio, R., and Horsfield, B., 2008, Tectonically induced adjustment of passive-margin accommodation space: influence on the hydrocarbon potential of the Orange Basin, South Africa, American Association of Petroleum Geologists Bulletin, v. 92, no. 5, p. 589—609, doi:10.1306/12280707023.

Pazzaglia, F.J. and Brandon, M.T., 1996, Macrogeomorphic evolution of the post-Triassic Appalachian mountains determined by deconvolution of the offshore basin sedimentary record, Basin Research, v. 8, no. 3, p. 255—278, doi:10.1046/j.1365-2117.1996.00274.x.

Pirmez, C., Pratson, L.F., and Steckler, M.S., 1998, Clinoform development by advection-diffusion of suspended sediment: Modeling and comparison to natural systems, Journal of Geophysical Research, v. 103, no. B10, p. 24141—24157, doi:10.1029/98JB01516.

Poag, C.W., 1992, U.S. Middle Atlantic continental rise: Provenance, dispersal, and deposition of Jurassic to Quaternary sediments, *in* Poag, C.W. and Graciansky, P.C., eds., Geologic Evolution of Atlantic Continental Rises: Springer, p. 100—156.

Poag, C.W. and Sevon, W.D., 1989, A record of Appalachian denudation in postrift Mesozoic and Cenozoic sedimentary deposits of the U.S. Middle Atlantic continental margin, Geomorphology, v. 2, no. 1—3, p. 119—157, doi:10.1016/0169-555X(89)90009-3.

Ramsay, P.J. and Cooper, J.A.G., 2002, Late Quaternary sea-level change in South Africa, Quaternary Research, v. 57, no. 1, p. 82—90, doi:10.1006/qres.2001.2290.

Rivenaes, J.C., 1992, Application of a dual-lithology, depth-dependent diffusion equation in stratigraphic simulation, Basin Research, v. 4, p. 133—146, doi:10.1111/j.1365-2117.1992.tb00136.x.

Rivenaes, J.C., 1997, Impact of sediment transport efficiency on large-scale sequence architecture: results from stratigraphic computer simulation, Basin Research, v. 9, p. 91—105, doi:10.1046/j.1365-2117.1997.00037.x.

Roering, J.J., Kirchner, J.W., and Dietrich, W.E., 1999, Evidence for nonlinear, diffusive sediment transport on hillslopes and implications for landscape morphology, Water Resources Research, v. 35, no. 3, p. 853—870, doi:10.1029/1998WR900090.

Ross, W.C., Halliwell, B.A., May, J.A., Watts, D.E., and Syvitski, J.P.M., 1994, Slope readjustment: A new model for the development of submarine fans and aprons, Geology, v. 22, p. 511—514, doi:10.1130/0091-7613(1994)022<0511:SRANMF>2.3.CO;2.

Rouby, D., Braun, J., Robin, C., Dauteuil, O., and Deschamps, F., 2013, Long-term stratigraphic evolution of Atlantic-type passive margins: A numerical approach of interactions between surface processes, flexural isostasy and 3D thermal subsidence, Tectonophysics, v. 604, p. 83—103, doi:10.1016/j.tecto.2013.02.003.

Sadler, P.M., 1981, Sediment accumulation rates and the completeness of stratigraphic sections, The Journal of Geology, v. 89, no. 5, p. 569—584, doi:10.1086/628622.

Salles, T., 2019, eSCAPE: Regional to global scale landscape evolution model v2.0, Geoscientific Model Development, v. 12, p. 4165—4184, doi:10.5194/gmd-12-4165-2019.

Salles, T. and Hardiman, L., 2016, Badlands: An open-source, flexible and parallel framework to study landscape dynamics, Computers & Geosciences, v. 91, p. 77—89, doi:10.1016/j.cageo.2016.03.011.

Salles, T., Ding, X., and Brocard, G., 2018, pyBadlands: A framework to simulate sediment transport, landscape dynamics and basin stratigraphic evolution through space and time, PLoS ONE, v. 13, no. 4, doi:10.1371/journal.pone.0195557.

Schanz, S.A., Montgomery, D.R., Collins, B.D., and Duvall, A.R., 2018, Multiple paths to straths: A review and reassessment of terrace genesis, Geomorphology, v. 312, p. 12—23, doi:10.1016/j.geomorph.2018.03.028.

Sclater, J.G. and Christie, P.A.F., 1980, Continental Stretching: An explanation of the Post-Mid-Cretaceous subsidence of the central North Sea Basin, Journal of Geophysical Research: Solid Earth, v. 85, no. B7, p. 3711—3739, doi:10.1029/JB085iB07p03711.

Shobe, C.M., Tucker, G.E., and Barnhart, K.R., 2017, The SPACE 1.0 model: a Landlab component for 2-D calculation of sediment transport, bedrock erosion, and landscape evolution, Geoscientific Model Development, v. 10, no. 12, p. 4577—4604, doi:10.5194/gmd-10-4577-2017.

Sisson, S.A., Fan, Y., and Tanaka, M.M. (2007) Sequential Monte Carlo without likelihoods, Proceedings of the National Academy of Sciences, v. 104, no. 6, p. 1760-1765, doi:10.1073/pnas.0607208104.

Steckler, M.S., Reynolds, D.J., Coakley, B.J., Swift, B.A., and Jarrad, R., 1993, Modelling passive margin sequence stratigraphy, *in:* Posamentier, H.W., Summerhayes, C.P., Haq, B.U., and Allen, G.P., eds., Sequence Stratigraphy and Facies Associations, p. 19—41, doi:10.1002/9781444304015.ch2.

Steckler, M.S., Swift, D.J.P., Syvitski, J.P., Goff, J.A., and Niedoroda, A.W., 1996, Modeling the sedimentology and stratigraphy of continental margins, Oceanography, v. 9, no. 3, p. 183—188.

Steckler, M.S., Watts, A.B., and Thorne, J.A., 1988, Subsidence and basin modeling at the U.S. Atlantic passive margin, *in:* Sheridan, R.E. and Grow, J.A., eds., The Atlantic Continental Margin, U.S.: Geological Society of America, The Geology of North America, v. 1—2, p. 399—416..

Stanley, J.R., Braun, J., Baby, G., Guillocheau, F., Robin, C., Flowers, R.M., Brown, R., Wildman, M., and Beucher, R., Constraining plateau uplift in southern Africa by combining thermochronology, sediment flux, topography, and landscape evolution modeling, Journal of Geophysical Research: Solid Earth, v. 126, no. 7, doi:10.1029/2020JB021243.

Straub, K.M., Duller, R.A., Foreman, B.Z., and Hajek, E.A., 2020, Buffered, incomplete, and shredded: The challenges of reading an imperfect stratigraphic record, Journal of Geophysical Research: Earth Surface, v. 125, no. 3, doi:10.1029/2019JF005079.

Syvitski, J.P.M., Smith, J.N., Calabrese, E.A., and Boudreau, B.P., 1988, Basin sedimentation and the growth of prograding deltas, Journal of Geophysical Research: Oceans, v. 93, no. C6, p. 6895—6906, doi:10.1029/JC093iC06p06895.

Syvitski, J.P.M. and Hutton, E.W.H., 2001, 2D SEDFLUX 1.0C:: an advance process-response numerical model for the fill of marine sedimentary basins, Computers & Geosciences, v. 27, no. 6, p. 731—753, doi:10.1016/S0098-3004(00)00139-4.

Talling, P.J., Summer, E.J., Masson, D.G., and Malgesini, G., 2012, Subaqueous sediment density flows: Depositional processes and deposit types, Sedimentology, v. 59, p. 1937—2003, doi:10.1111/j.1365-3091.2012.01353.x.

Thran, A.C., East, M., Webster, J.M., Salles, T., and Petit, C., 2020, The influence of carbonate platforms on the geomorphological development of a mixed carbonate-siliciclastic margin (Great Barrier Reef, Australia), *Geochemistry, Geophysics, Geosystems*, v. 21, doi:10.1029/2020GC008915.

Toni, T., Welch D., Strelkowa, N., Ipsen, A., and Stumpf, M.P.H., 2009, Approximate Bayesian computation scheme for parameter inference and model selection in dynamical systems, Journal of the Royal Society Interface, v. 6, p. 187-202, doi:10.1098/rsif.2008.0172.

Valla, P.G., van der Beek, P.A., and Lague, D., 2010, Fluvial incision into bedrock: Insights from morphometric analysis and numerical modeling of gorges incising glacial hanging valleys (Western Alps, France), Journal of Geophysical Research: Earth Surface, v. 115, no. F2, doi:10.1029/2008JF001079.

Yanites, B.J., Becker, J.K., Madritsch, H., Schnellmann, M., and Ehlers, T.A., 2018, Lithologic effects on landscape response to base level changes: A modeling study in the context of the Eastern Jura Mountains, Switzerland, Journal of Geophysical Research: Earth Surface, v. 122, p. 2196—2222, doi:10.1002/2016JF004101.

Yuan, X.P., Braun, J., Guerit, L., Simon, B., Bovy, B., Rouby, D., Robin, C., and Jiao, R., 2019a, Linking continental erosion to marine sediment transport and deposition: A new implicit and *O(N)* method for inverse analysis, Earth and Planetary Science Letters, v. 524, doi:10.1016/j.epsl.2019.115728.

Yuan, X.P., Braun, J., Guerit, L., Rouby, D., and Cordonnier, G., 2019b, A new efficient method to solve the stream power law model taking into account sediment deposition, Journal of Geophysical Research: Earth Surface, v. 124, p. 1346—1365, doi:10.1029/2018JF004867.

Zhang, J., Sylvester, Z., and Covault, J., 2020, How do basin margins record long-term tectonic and climatic changes? Geology, v. 48, no. 9, p. 893—897, doi:10.1130/G47498.1.

**APPENDIX**

- Supporting table S1: parameters for PyABC ABC-SMC algorithm.
- Supporting table S2: parameter ranges and best-fit misfit values for inversions constrained by comparison against only the modern bathymetric surface.
- Supporting table S3: parameter ranges and best-fit misfit values for inversions constrained by comparison against the modern bathymetric surface and all subsurface reflectors.
- Supporting figure S4: inversion results from nonlocal, nonlinear model constrained by comparison against the modern bathymetric surface and all subsurface reflectors.
- Supporting figure S5: comparison between measured and modeled stratigraphy using the best-fit nonlocal, nonlinear model when constrained by comparison against the modern bathymetric surface and all subsurface reflectors.
- Supporting figure S6: inversion results from local, linear model constrained by comparison against the modern bathymetric surface and all subsurface reflectors.
- Supporting figure S7: comparison between measured and modeled stratigraphy using the best-fit local, linear model when constrained by comparison against the modern bathymetric surface and all subsurface reflectors.

**Supporting table S1: parameters for PyABC ABC-SMC algorithm.**

| Parameter | Inversion of nonlocal, nonlinear model | Inversion of local, linear model |
|---|---|---|
| Population size[1] | 300 | 100 |
| Number of populations[2] | 15 | 15 |
| Minimum misfit[3] | 0.01 | 0.01 |

1: A larger population size was used for the nonlocal, nonlinear model because this model had twice as many parameters to optimize. Population size does not enforce the number of model realizations that get run in any single generation; it enforces the number of "acceptable" models that are required to move to the next generation. Our experience was that the total number of model realizations was typically 3-4x greater than the product of the population size and the number of populations.

2: This represents the maximum number of populations that will run if the minimum misfit is not reached. We chose to set the minimum misfit unrealistically low so that we would have a consistent number of populations between our different inverse analyses.

3: When the minimum misfit is reached, the inversion stops even if the number of populations has not been reached. We therefore set the minimum misfit close to zero so that we would have a consistent number of populations between our different inverse analyses.

**Supporting table S2: parameter ranges and resulting maximum and minimum misfit values for models constrained using only the modern bathymetric surface.**

| | Nonlocal, nonlinear model | | | | | Local, linear model | | |
|---|---|---|---|---|---|---|---|---|
| **Sec.** | $\lambda$ **[m]** | $S_c$ **[-]** | $K$ **[m/yr]** | $z_*$ **[m]** | $\mu$ **[-]** | $K$ **[m/yr]** | $z_*$ **[m]** | $\mu$ **[-]** |
| **1** | (250000, 450000) | (0.08, 0.17) | ($10^{-3}$, $10^{2}$) | (1, 200) | **(51.8, 65.2)** | ($10^{-5}$, $10^{4}$) | (1, 40000) | **(47.9, 114.7)** |
| **3** | (100000, 300000) | (0.01, 0.1) | ($10^{-3}$, $10^{2}$) | (1, 200) | **(17.0, 131.4)** | ($10^{-5}$, $10^{1}$) | (250, 40000) | **(46.7, 309.6)** |
| **4** | (100000, 300000) | (0.01, 0.1) | ($10^{-3}$, $10^{2}$) | (1, 200) | **(20.3, 78.8)** | ($10^{-5}$, $10^{3}$) | (250, 40000) | **(34.5, 228.0)** |
| **5** | (100000, 300000) | (0.01, 0.1) | ($10^{-3}$, $10^{2}$) | (1, 200) | **(11.1, 78.8)** | ($10^{-5}$, $10^{3}$) | (150, 40000) | **(37.1, 199.0)** |
| **6** | (100000, 300000) | (0.01, 0.1) | ($10^{-3}$, $10^{2}$) | (1, 200) | **(14.1, 94.9)** | ($10^{-5}$, $10^{3}$) | (150, 40000) | **(34.0, 249.4)** |
| **7** | (200000, 400000) | (0.01, 0.1) | ($10^{-3}$, $10^{2}$) | (1, 200) | **(28.1, 94.1)** | ($10^{-5}$, $10^{3}$) | (250, 40000) | **(47.5, 289.2)** |
| **8** | (150000, 350000) | (0.01, 0.1) | ($10^{-3}$, $10^{2}$) | (1, 200) | **(15.5, 92.2)** | ($10^{-5}$, $10^{3}$) | (250, 40000) | **(38.3, 254.3)** |

**Supporting table S3: parameter ranges and resulting maximum and minimum misfit values for models constrained using the modern bathymetric surface and all subsurface reflectors.**

| | **Nonlocal, nonlinear model** | | | | | **Local, linear model** | | |
|---|---|---|---|---|---|---|---|---|
| **Sec.** | $\lambda$ **[m]** | $S_c$ **[-]** | $K$ **[m/yr]** | $z_*$**[m]** | $\mu$ **[-]** | $K$ **[m/yr]** | $z_*$**[m]** | $\mu$ **[-]** |
| **1** | (200000, 400000) | (0.08, 0.17) | ($10^{-3}$, $10^{2}$) | (1, 200) | **(82.0, 85.2)** | ($10^{-5}$, $10^{3}$) | (1, 40000) | **(86.1, 108.4)** |
| **3** | (100000, 300000) | (0.01, 0.1) | ($10^{-3}$, $10^{2}$) | (1, 200) | **(91.3, 147.5)** | ($10^{-5}$, $10^{3}$) | (1, 40000) | **(109.4, 275.9)** |
| **4** | (150000, 350000) | (0.01, 0.1) | ($10^{-3}$, $10^{2}$) | (1, 200) | **(82.2, 100.6)** | ($10^{-5}$, $10^{3}$) | (1, 40000) | **(97.9, 190.4)** |
| **5** | (100000, 300000) | (0.01, 0.1) | ($10^{-3}$, $10^{2}$) | (1, 200) | **(76.3, 103.6)** | ($10^{-5}$, $10^{3}$) | (1, 40000) | **(96.4, 165.1)** |
| **6** | (150000, 350000) | (0.01, 0.1) | ($10^{-3}$, $10^{2}$) | (1, 200) | **(84.1, 102.3)** | ($10^{-5}$, $10^{3}$) | (1, 40000) | **(104.0, 188.2)** |
| **7** | (250000, 450000) | (0.01, 0.1) | ($10^{-3}$, $10^{2}$) | (1, 200) | **(91.8, 108.8)** | ($10^{-5}$, $10^{3}$) | (1, 40000) | **(121.5, 232.3)** |
| **8** | (200000, 400000) | (0.01, 0.1) | ($10^{-3}$, $10^{2}$) | (1, 200) | **(83.7, 100.5)** | ($10^{-5}$, $10^{3}$) | (1, 40000) | **(105.0, 198.3)** |

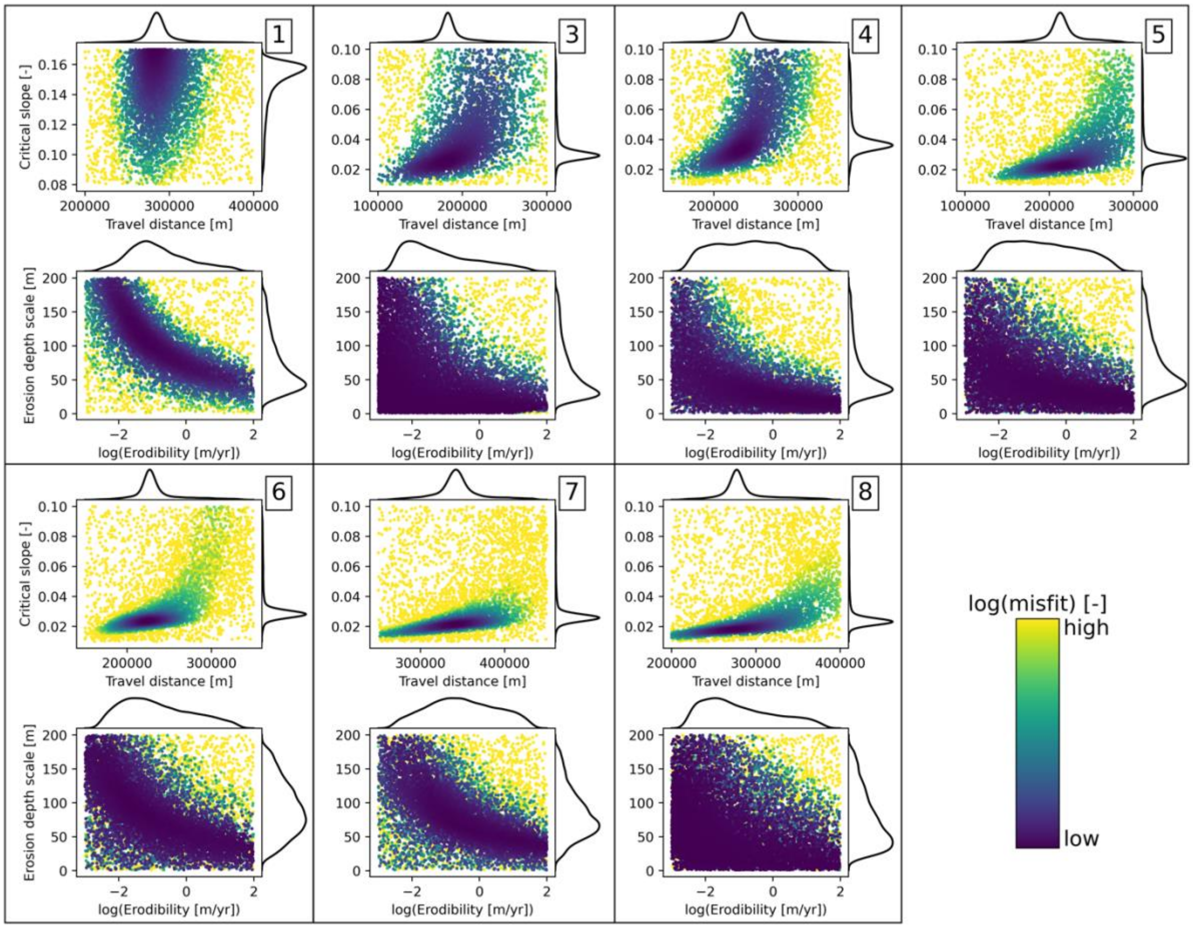


**Supporting figure S4: Results for all seven sections from the search for a best-fit parameterization of the nonlocal, nonlinear model with the inversion procedure constrained using the modern bathymetric surface and all subsurface reflectors. Scatter plots show model-data misfit (color) as a function of the four key parameters. Kernel density estimate (KDE) plots show the distribution of values for each parameter. Because the inversion procedure runs more model realizations in regions of the parameter space with reduced model-data misfit, peaks in the KDE plots can be interpreted as showing the region of each parameter's range that leads to the lowest misfit. Narrow peaks in the KDE plots indicate parameters with well-constrained best-fit values, while broad peaks indicate parameters for which a wide range of values produces similar misfit. Numbered sets of plots refer to the seismic section used for the inversion. Maximum and minimum misfit values vary between sections; color values have been scaled for maximum interpretability.**

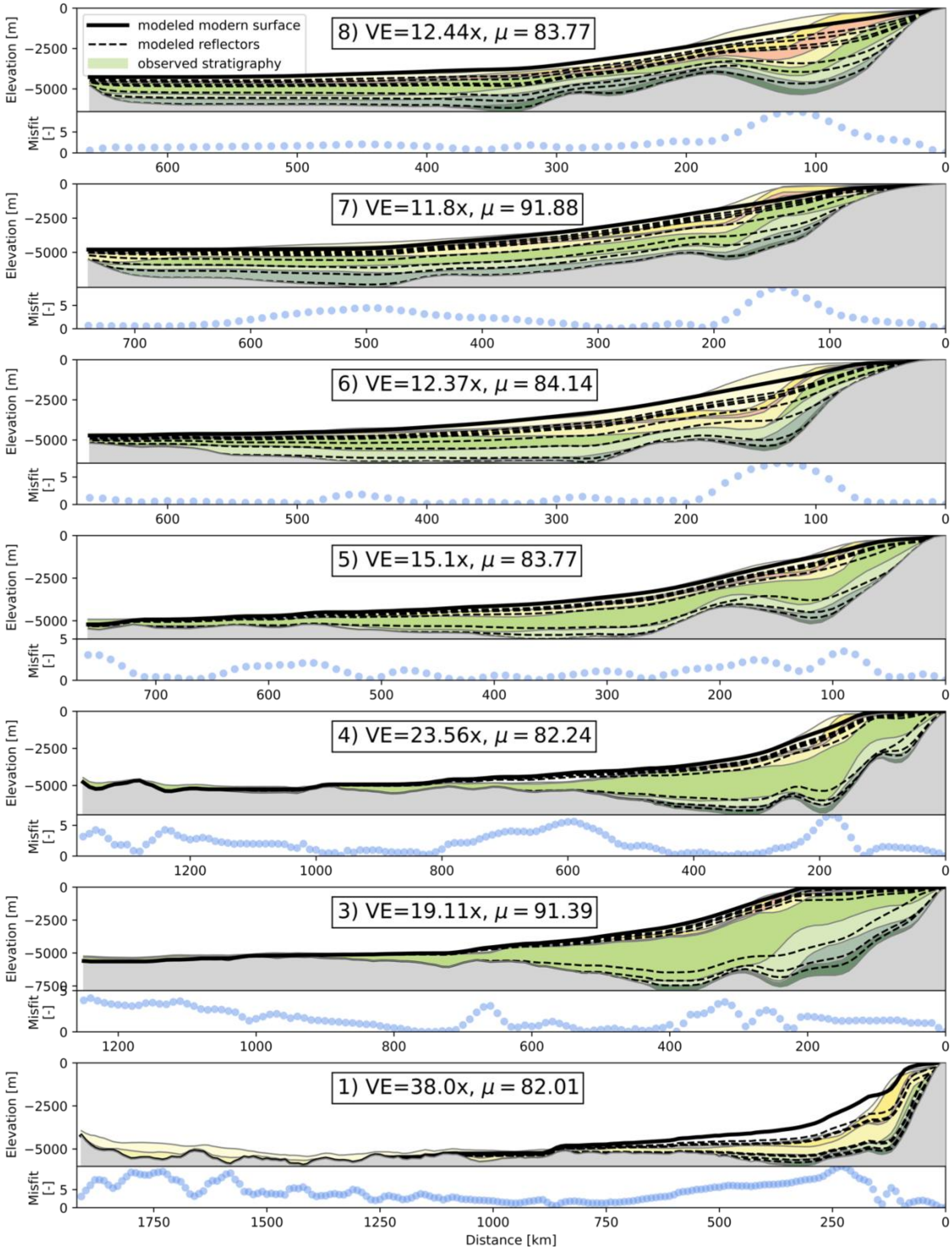


**Supporting figure S5: Comparison between modeled and measured stratigraphy using the nonlocal, nonlinear model for all seven sections when both the modern bathymetric surface and all subsurface reflectors were used to assess fit. VE is vertical exaggeration.**

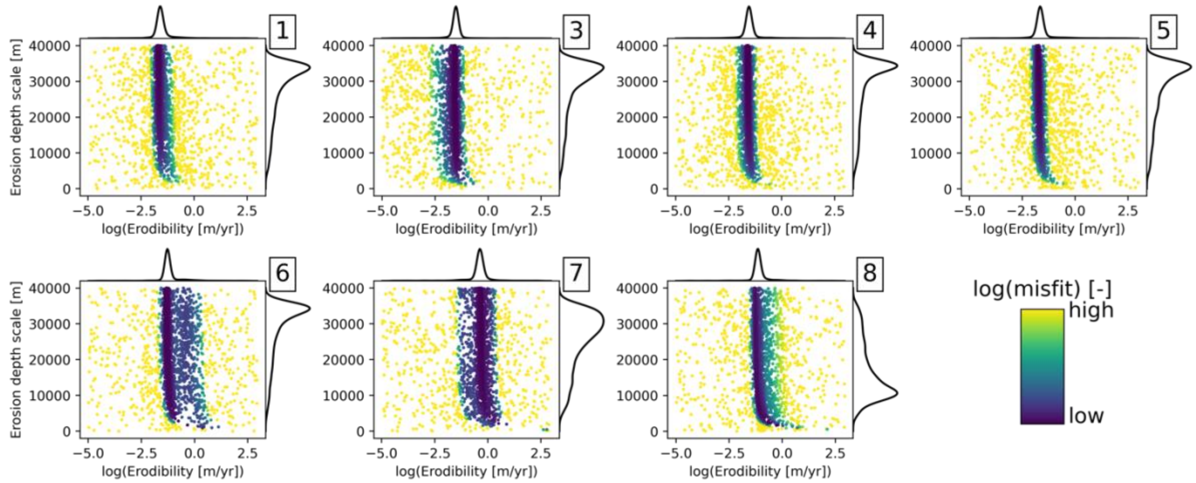


**Supporting figure S6: Results for all seven sections from the search for best-fit parameter values for the local, linear diffusion model with the inversion procedure constrained using the modern bathymetric surface and all subsurface reflectors.**

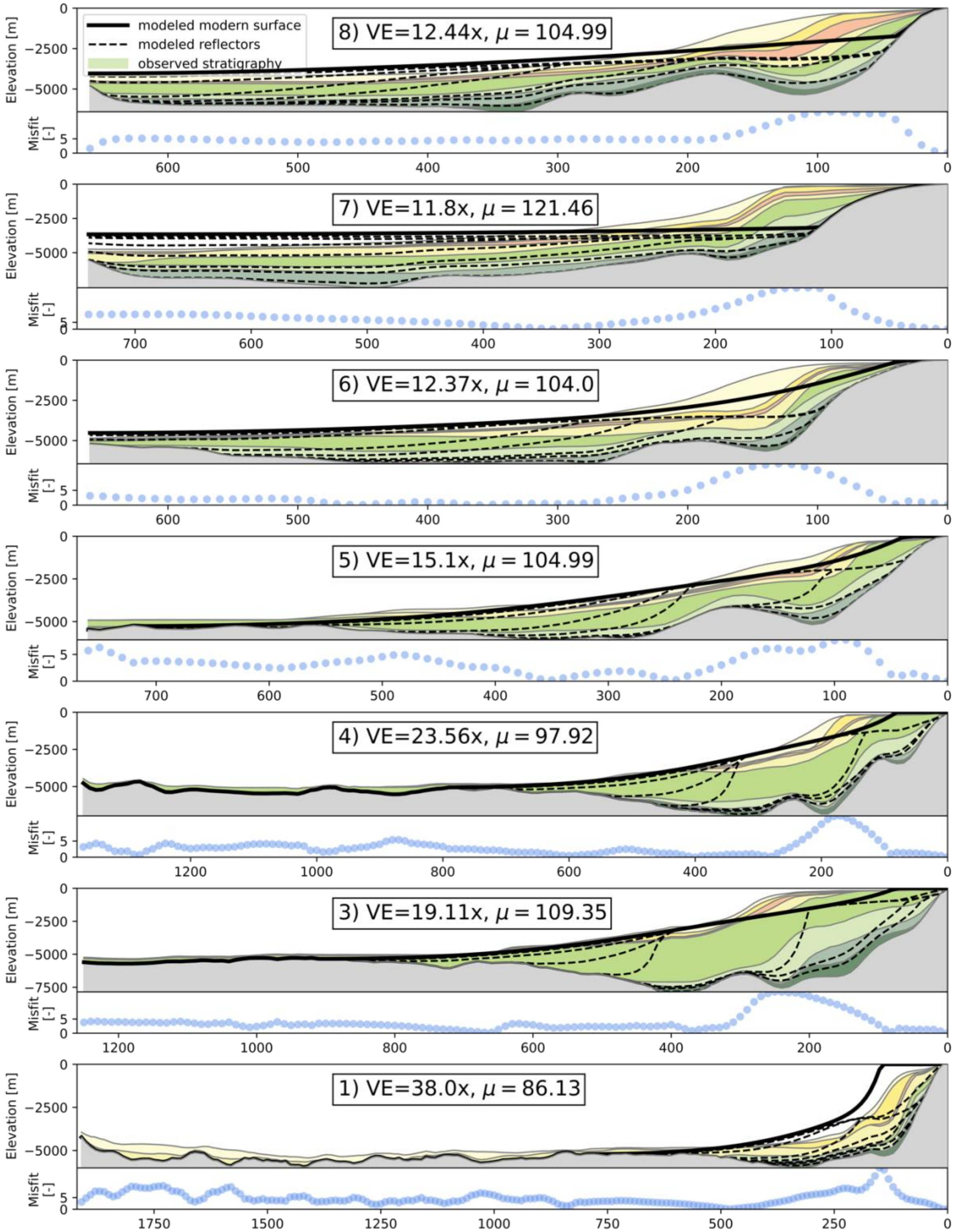


**Supporting figure S7: Comparison between modeled and measured stratigraphy using the local, linear model for all seven sections when both the modern bathymetric surface and all subsurface reflectors were used to assess fit. VE is vertical exaggeration.**